

# **Influence of Boulders on Channel Width and Slope: Field Data and Theory**

Ron Nativ<sup>1,2,3</sup>, Jens M. Turowski<sup>3</sup>, Liran Goren<sup>1</sup>, Jonathan B. Laronne<sup>4</sup> and J. Bruce H. Shyu<sup>5</sup>

<sup>1</sup>Department of Earth and Environmental Sciences, Ben-Gurion University of the Negev, Israel

<sup>2</sup>University of Potsdam, Institute of Earth and Environmental Science, Potsdam, Germany

<sup>3</sup>GeoForschungsZentrum, Helmholtz Centre Potsdam, Potsdam, Germany

<sup>4</sup>Department of Geography and Environmental Development, Ben-Gurion University of the Negev, Israel

<sup>5</sup>Department of Geosciences, National Taiwan University, Taipei, Taiwan

*Correspondence to:* Ron Nativ ([ronnat@post.bgu.ac.il](mailto:ronnat@post.bgu.ac.il))

## **Abstract**

Large boulders with a diameter of up to several tens of meters are globally observed in mountainous bedrock channel environments. Recent theories suggest that high concentrations of boulders are associated with changes in channel morphology. However, data are scarce and ambiguous, and process-related studies are limited. Here we present data from the Liwu River, Taiwan, showing that channel width and slope increase with boulder concentration. We apply two mass balance principles of bedrock erosion and sediment transport and develop a theory to explain the steepening and widening trends. Five mechanisms are considered and compared to the field data. The cover effect by immobile boulders is found to have no influence on channel width. Channel width can partially be explained by boulder control on the tools effect and on the partitioning of the flow shear stress. However, none of the mechanisms we explored can adequately explain the scattered width data, potentially indicating a long-timescale adjustment of channel width to boulder input. Steepening can be best described by assuming a reduction of sediment transport efficiency with boulder concentration. We find that boulders represent a significant perturbation to the fluvial landscape. Channels tend to adjust to this perturbation leading to a new morphology that differs from boulder-free channels. The general approach presented here can be further expanded to explore the role of other boulder-related processes.

## **Key Points**

- Reach-scale bedrock channel width and sediment-bed slope increase with boulder-concentration in the Liwu River, Taiwan.
- Reduction of transport efficiency due to boulders best explains the increase in slope in boulder-bed channels.

- Models incompatibility to account for scattered width data could imply long adjustment time scale to boulder input.

### **Plain Language Summary**

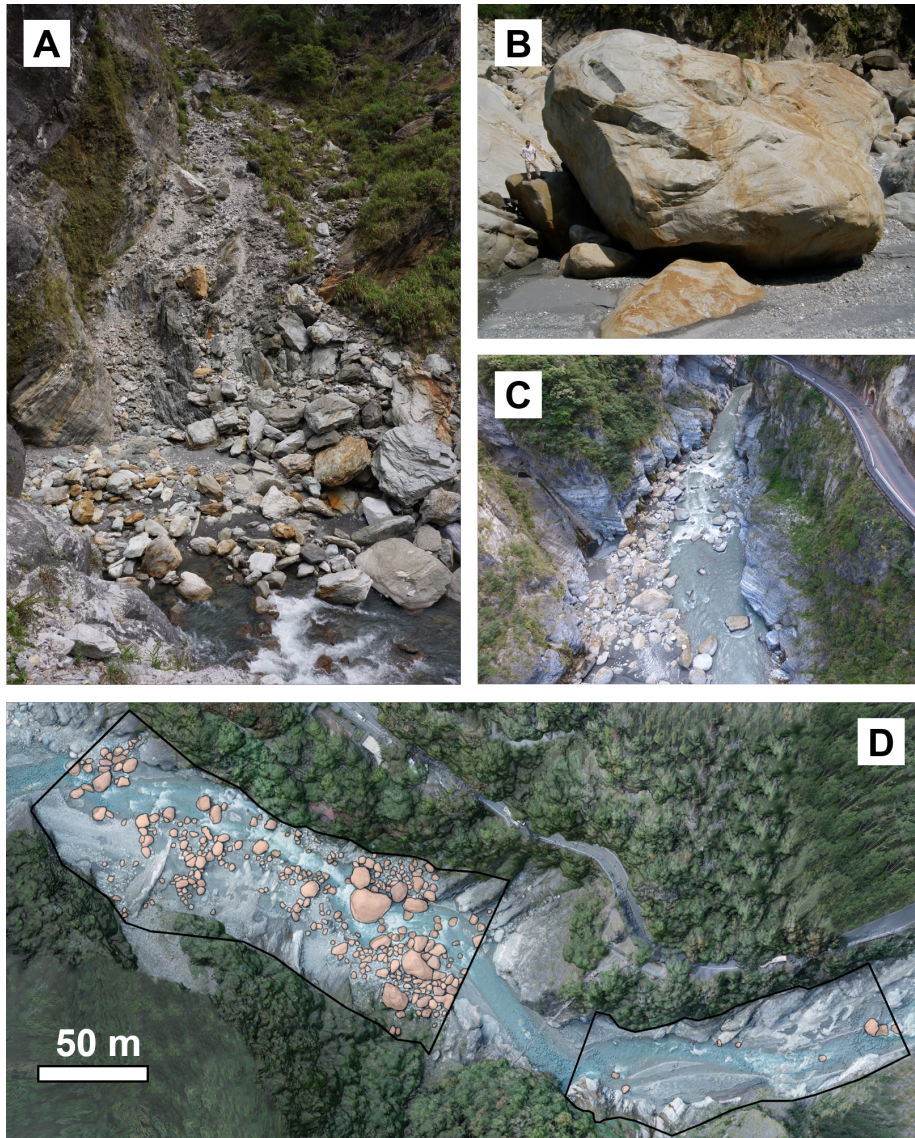
Boulders are significant features in mountainous landscapes and can be found on hillslopes and river beds. The Liwu River, Taiwan, exhibits boulders with sizes of tens of meters, which are probably rarely mobile during floods. Channel segments that host large concentrations of boulders are generally wider and steeper, offering an opportunity to examine the roles of boulders in shaping the geometry of the channel. Here we use two fundamental principles related to the mass balance of (1) the riverbed rock eroded by pebble impacts and (2) pebble transport downstream during floods to develop a set of equations that predict the slope and width behavior as a result of boulder presence. The increase of slope with more boulders can be explained by assuming that high concentrations of boulders inhibit the rate of the transported pebbles by causing them to, for example, take longer paths. A fraction of the scattered width data can be accounted for by increasing friction forces between the water flow and boulders and by increasing the rate of sediment impact between boulders due to a reduction in the free riverbed space. This work demonstrates the significant role of boulders in shaping landscapes.

## **Introduction**

Boulders are ubiquitous in mountainous landscapes responding to large magnitude tectonic perturbations and extreme variability of climatic conditions (Shobe et al., 2021). Boulders with a wide range of diameters, between tens of centimeters and a few tens of meters, can be found on hillslopes (e.g., Bennett et al., 2016; Finnegan et al., 2019; Shobe et al., 2020) and in rivers (e.g., Bathurst, 1996; Pagliara and Chiavaccini, 2006)(Fig. 1). While the definition of a boulder varies among different studies, here boulders are defined as the largest and least mobile grains in a landscape (Shobe et al., 2021). Much focus has been given to the effects of small to intermediate size boulders, with diameters of tens of centimeters to few meters, on channel hydraulics, channel geometry, and sediment transport (e.g., Carling et al., 2002; Nitsche et al., 2011). Small to intermediate size boulders are commonly found in steep alluvial channels such as cascades and step-pools (Montgomery and Buffington, 1997) and in mountainous torrents, where they are thought to play a significant role in modifying bedload transport rates and patterns (Yager et al., 2007; Nitsche et al., 2011; Rickenmann and Recking, 2011), flow structure and velocity (Canovaro et al., 2007; Nitsche et al., 2012) and channel bed roughness (e.g., Schneider et al., 2015; Johnson, 2017).

A series of recent studies explored the morphological effects of larger boulders, a few meters and more in diameter, which are more common in bedrock rivers (Cook et al., 2018; Shobe et al., 2020, 2021). Such large boulders have been

argued to be immobile for prolonged durations with expected substantial impacts on channel hydraulics and channel geometry and long-term geomorphic functionality (Haviv, 2007; Huber et al., 2020; Shobe et al., 2021). The emplacement of large boulders is associated with glacial lake outburst floods (Cook et al., 2018), rockfalls, debris flows, landslides, and glacial erratics (e.g., Jouvét et al., 2017; Polvi, 2021). In addition to their hypothesized effects on landscape evolution (e.g., Shobe et al., 2016), the role of boulders as geohazards (Kean et al., 2019; Dini et al., 2021; Shobe et al., 2021) has recently been recognized. Like changes in tectonics and climate, boulder emplacement in rivers can be regarded as a disturbance to the fluvial system, forcing its geometry to adjust in response to the new hydraulic conditions set by the large boulders. Boulders may affect the scaling relations between channel steepness and catchment-scale erosion rate (Shobe et al., 2018) in comparison to those expected for boulder-free channels (e.g., Lague et al., 2005; DiBiase et al., 2010; DiBiase and Whipple, 2011). Despite these recent insights, the effects of large immobile boulders on channel geometry, especially channel width, have not been systematically studied, and the processes involved in channel geometrical modifications in response to large boulders emplacement have mostly remained unexplored.



Here, we explore the hypothesis that increasing boulder concentration can cause channels to widen and steepen. We collected field data of channel geometry, morphology, and boulder characteristics. The data are based on field and remote sensing observations from the Liwu River in Taiwan, where boulders with diameters of up to meters are ubiquitous on the channel bed along various river reaches, differing in drainage area and geometry. Our goals are to (1) study the relationship between channel slope, width, and boulder concentration and (2) theoretically identify the processes linking these variables. To achieve the second goal, we focus on the influence of boulders on bedrock erosion and sediment

transport and describe their effects using conceptual arguments and empirical relations. We establish a suite of mechanisms that relate immobile boulders to bedrock channels' steady-state width and slope. We treat each mechanism independently, discuss the trends it predicts, and compare them against field observations. In the following, we review the literature concerning flow hydraulics induced by boulders, the effects of boulders on sediment transport processes, and the state-of-the-art regarding the channel adjustments in the presence of large boulders.

## **Background for Boulder Control on Channel Geometry**

### **Boulder Effects on Hydraulics and Sediment Transport**

Boulders are macro-roughness elements, which enhance flow resistance and alter the flow structure (Nitsche et al., 2011). For example, in mountain streams with relatively shallow flows, boulders exert drag forces on the flow, violating the classic view of a logarithmic velocity profile (e.g., Wiberg and Smith, 1991; Canovaro et al., 2007). Due to the complex three-dimensional flow structure, the spatial distribution of shear stresses significantly varies in the vicinity of boulders, causing local variations in sediment transport (Papanicolaou et al., 2012; Papanicolaou and Tsakiris, 2017). Boulders modify flow patterns around them, such as turbulence intensity, and promote flow accelerations and decelerations (e.g., Tsakiris et al., 2014). In high relative submergence flows, where the water depth is much greater than the boulder diameter, the near-wake zone of a boulder becomes a zone of flow reversals and decelerations (e.g., Dey et al., 2011). It is, thus, expected that such flow regimes favor sediment deposition and clustering downstream of boulders (e.g., Papanicolaou and Kramer, 2006).

Boulders and large clasts are thought to reduce the available shear stress for sediment motion (e.g., Buffington and Montgomery, 1997). Coupling theory and flume experiments, Yager et al. (2007) suggested that the drag exerted by immobile boulders could explain why traditional transport equations overpredict bedload fluxes by orders of magnitude. Canovaro et al. (2007) designed flume experiments with different portions of boulder concentrations, demonstrating a humped relationship between the percentage of drag and total shear stress versus boulder concentration. For small boulder concentration values, the drag force increased logarithmically until it peaked. The drag force decreased linearly with a further boulder concentration increase until it dropped to zero when boulders fully covered the bed. With the strong dependence of bedload transport on the available shear stress (e.g., Nitsche et al., 2011), these results strengthen the contention that bedload flux is reduced in boulder-bed channels.

## Boulder-bed Bedrock Channels and Relationships with Channel Slope and Width

Various studies reported links between boulders and channel morphology (e.g., Montgomery and Buffington, 1997; Lenzi, 2001; Turowski et al., 2009b; Thaler and Covington, 2016; Cook et al., 2018; Shobe et al., 2018, 2020). Recent investigations identified a positive relationship between boulders and channel steepness (Thaler and Covington, 2016) and slope (Shobe et al., 2020) in bedrock channels. Steady-state bedrock channel morphology is assumed to control long-term river bedrock erosion adjustment to the long-term uplift rate (e.g., Whipple and Tucker, 1999). When the uplift rate changes, the erosion rate responds by adjusting the river profile (e.g., Whipple, 2004; Lague et al., 2005) and cross-section geometry (e.g., Turowski et al., 2009a; Yanites, 2018; Turowski, 2020). Assuming immobility of large boulders, Shobe et al. (2020) exploited this notion to argue that boulders hinder erosion by protecting the bedrock channel bed. Their model predicts that a boulder-bed channel would consequently steepen to compensate for the reduced erosion. Immobile boulders were also argued to be consequential for changes in bedrock channel width. Shobe et al. (2020) tested the influence of the proximity of the boulder delivery point (e.g., landslides scars) on the width coefficient, i.e., width normalized by drainage area (e.g., Lague, 2014) and found contrasting results. Accordingly, conclusive data and a general theory of boulder influence on bedrock channel width are still missing.

Understanding how boulders influence channel morphology in bedrock rivers requires insights into the process of bedrock erosion and sediment transport. The slope of bedrock channels has been argued to adjust to both bedrock erosion requirement and the mobilization of upstream sediment supply (e.g., Sklar and Dietrich, 2006). However, the degree to which slope adjusts to each of these components remains unclear (Johnson et al., 2009). While channel slope is commonly considered to be the consequence of bedrock erosion and reshaping of the long profile (e.g., Royden and Perron, 2013), recent studies suggest that equilibrium of bedrock channels could be attained by a modification of the slope of sediment overlying the bedrock (Phillips and Jerolmack, 2016; Turowski, 2020, 2021). As in alluvial channels, rearrangement of the bed to form a new sediment-bed slope can be achieved via selective deposition and entrainment processes during floods (Mackin, 1948; Schumm and Parker, 1973; Schneider et al., 2015b; Turowski and Hodge, 2017), which relates to sediment transport processes. Furthermore, adjusting sediment-bed slope can be achieved within a timescale of a single flood, significantly faster than the timescale associated with bedrock erosion and the formation of a new bedrock slope (Turowski, 2020).

In abrasion-dominated channels, erosion of the bedrock bed and banks are thought to occur during flood events and are driven by impacts of sediment grains, which travel as bedload (e.g., Sklar and Dietrich, 2004; Cook et al., 2013; Auel et al., 2017). Channel widening occurs by lateral erosion, which is thought to be a consequence of sediment particles deflected to the sides following encounters with bed roughness elements (e.g., Li et al., 2020). A field study

from a bedrock channel gorge in Switzerland showed that wall erosion increases in proximity to roughness elements (Beer et al., 2017). Although recent studies proposed a positive relationship between channel roughness and lateral erosion (Fuller et al., 2016; Turowski, 2018; Li et al., 2020; He et al., 2021) the precise nature of this relationship remains to be explored (Turowski, 2020).

In the light of the above review, adjustment of channel width and slope to perturbations caused by immobile boulders can be expected to be controlled by bedrock erosion and sediment transport processes. Changing channel slope could occur by eroding the bedrock bed and altering sediment cover and depth by sediment deposition and entrainment. In contrast, existing models and observations indicate that widening the channel is only possible by lateral erosion. Due to the estimated long timescales of width adjustment (see below)(Turowski, 2020), a link between steady-state width and boulder concentration can be established if we consider at least one of the following conditions. First, the timescale of bedrock channel width adjustment to boulder input is shorter than the residence time of boulders within a river. Theoretically, the widening of bedrock channels such as the Liwu River is expected to extend to periods of up to thousands of years. Second, boulder supply and boulder degradation balance each other to keep the concentration of boulders steady over the required time scale for width adjustment. These assumptions will be reviewed in the discussion.

## **Boulders and Channel Morphology in the Liwu River: Methods and Empirical Data**

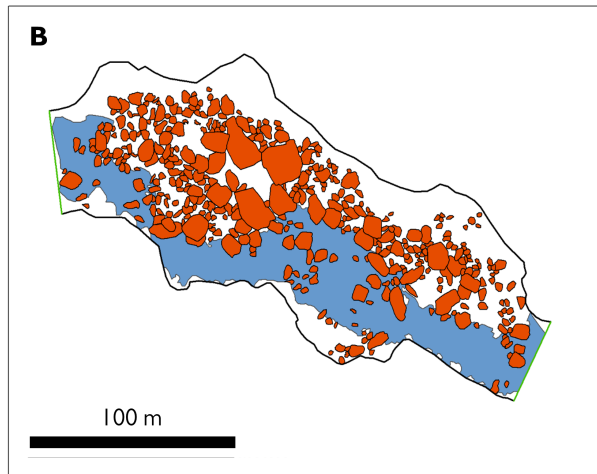
The Liwu River, Taiwan, exhibits numerous fluvial bedrock reaches hosting huge boulders. This section describes the methods applied for data collection in the Liwu River (Section 2.1) and empirical relations of boulder concentration and channel slope and width based on these data (Section 2.2).

### **Data Collection**

We documented 20 fluvial reaches along the Liwu River. Field data were collected in field campaigns during the low flow seasons of 2018 and 2019. We selected different fluvial reaches with variable drainage areas and local relief, representing various portions of the drainage basin. Our primary focus was on reaches with a substantial number of boulders, but we also collected data from reaches with lower boulder concentrations. We avoided fluvial reaches with incoming tributaries to ensure a minimal difference in drainage area within a given reach. To avoid lithology differences, we used a geological map of Taiwan to verify that the lithology does not change within the selected reaches. We avoided reaches exhibiting a large spatial variability in channel width. In each channel reach, a drone was used to document the channel at 80 - 120 m above the channel, constrained by the complexity of the topography and the pilot's

location. The channel bed and banks were photographed primarily at vertical and various other angles, with ~80% overlapping area. Due to the steep topography of many bedrock canyon sections, most of the reaches were inaccessible by foot, thus prohibiting emplacement of Ground Control Points (GCPs). We generated point clouds from the photos by using the AGISOFT METASHAPE commercial software. We created orthophotos and DEMs at 5 - 25 cm/pixel horizontal spatial resolutions, depending on the site and data quality. To account for the elevation uncertainty associated with the output models, we assume an elevation error of  $\pm 0.5$  m for the DEM.

The reach area  $A_{tot}$  was manually delineated using a digitization process in ArcGIS. First, the upstream and downstream channel reach boundaries were chosen and delineated with straight lines, bounding what we observed as a continuous distribution of boulders (Fig. 2). Second, the channel bank boundaries were identified and tracked by following distinctive bedrock-vegetation contacts. To evaluate the boulder-concentration in the channel reach, we manually digitized the map-view area of all of the visible boulders with an average diameter  $\geq 2$  m (Fig. 2B). A boulder was commonly recognized by observing that it protrudes from either water or a gravel bar. Boulder-concentration was calculated using the relation  $\Gamma = A_b/A_{tot}$ , where  $A_b$  is the sum of the areas of all of the boulders and can range between zero and one. To extract boulder diameters from the delineated map-view polygons, we assumed that boulders are circles. Reach-averaged channel width  $W_b$  was calculated using two methods: (1) by dividing the reach area by the thalweg length  $L$ , the assumed streamwise distance that follows the curvature of the map-view channel banks, and we consider a 5 m uncertainty on the measurement of  $L$ . (2) By manually measuring ten bank-to-bank lengths, perpendicular to channel banks, along the reach and using the average as a representative. We calculated the Root Mean Square Error (RMSE) value between the two methods to be 3.4 m (5% of the average reach width measurements in all reaches). The standard deviation (STD) of each ten measurements was used as an error on channel width measurements. To calculate reach-scale channel slope  $S_b$  in a boulder-bed channel, the cross-sections that define the upstream and downstream boundaries of the reach area (Fig. 2) were extracted from the DEM. The minimum elevation point of each cross-section was subtracted and divided by  $L$ . Because a substantial fraction of the bedrock bed is occupied with fine sediments, the slope represents a sediment-bed slope, which might differ from the bedrock-bed slope.



Theory and global observations show that to first order and in the absence of other perturbations, channel width increases (e.g., Montgomery and Gran, 2001; Whitbread et al., 2015) and slope decreases (e.g., Wobus et al., 2006) with drainage area. Consequently, to isolate the effects of boulders, the impact of the drainage area needs to be removed. We use a dimensionless width ratio  $W_b/W$ , defined as the average width ratio of paired reaches located immediately upstream or downstream from one another, presumably without tributaries joining between them.  $W_b$  refers to the measured width of a boulder-bed channel, and  $W$  refers to the width of a boulder-free channel. Similarly, we define a slope ratio  $S_b/S$ . Each selected pair of reaches shares a similar drainage area and lithology. Calculations of boulder-free width  $W$  were performed using two approaches. First, the average of ten measurements exploiting Google-Earth imagery, and second, utilizing a basin-wide scaling relationship between width and drainage area for boulder-free channels (Fig. S). The first approach can test local width anomalies compared to the standard width derived using the second approach. Data points that show significant difference between the two methods are suspected of experiencing a local effect on width. Channel reaches with a large discrepancy between the two measurements are marked differently in plots. The boulder-free slope  $S$  was determined by a power-law regression between channel slope versus drainage area (Fig. S) based on data of channels with minor boulder presence.

## Empirical Relations

The collected data include channel reaches with widths ranging between 30 and 120 m, slopes ranging from 0.01 to over 0.08, and boulder concentrations that range between  $\sim 0$  and 0.34 (Table 1; Fig. 3). We observe that both channel width (Fig. 3A;  $R^2 = 0.29$ ) and slope (Fig. 3B;  $R^2 = 0.51$ ) tend to increase with boulder concentration  $\Gamma$ . The two approaches for evaluating boulder-free width  $W$  are compared (Fig. S2) and yield relatively similar width ratios; among 20 data points, only two lie outside a 50% error. A comparison between the methods yields a Root Mean Square Error (RMSE) value of 0.46, or 0.22 if the two outliers are excluded. The width ratio  $W_b/W$  (Fig. 3D;  $R^2 = 0.42$ ) and slope ratio,  $S_b/S$  ( $R^2 = 0.71$ ) increase with boulder concentration. In both cases, normalization by using the paired boulder-free reach improves the relationship with  $\Gamma$ , as indicated by an increase of the  $R^2$  (Fig. 3). Although the width ratio exhibits scatter for a given  $\Gamma$ ,  $W_b/W$  is always larger than one for  $\Gamma > 0.05$ . Over a range of 35% variability in boulder-concentration, the slope ratio increases from about unity to  $> 4$ .

**Table 1:** Liwu River data

Maximal boulder size $D_{\max}$ [m]	Mean boulder size $D_{\text{mean}}$ [m]	Boulder-concentration,	<sup>d</sup> Slope
6.2	2.9	0.05	0.33
7.5	4.0	0.10	0.78
12.2	3.3	0.04	1.28

Maximal boulder size $D_{\max}$ [m]	Mean boulder size $D_{\text{mean}}$ [m]	Boulder-concentration,	<sup>d</sup> Slope
19.5	4.4	0.34	3.01
15.4	4.0	0.17	1.61
9.1	2.0	0.07	0.96
7.9	2.6	0.09	1.63
15.2	4.1	0.29	2.72
5.5	3.4	0.03	1.06
10.4	1.7	0.05	1.27
7.1	3.4	0.02	1.02
17.2	2.6	0.24	1.96
23.4	4.4	0.22	1.53
12.4	3.3	0.15	1.85
3.6	2.2	0.01	0.55
23.2	3.5	0.16	1.30
19.1	3.0	0.29	3.59
12.2	2.1	0.10	0.94
17.3	3.3	0.20	2.59
19.2	2.5	0.16	1.85

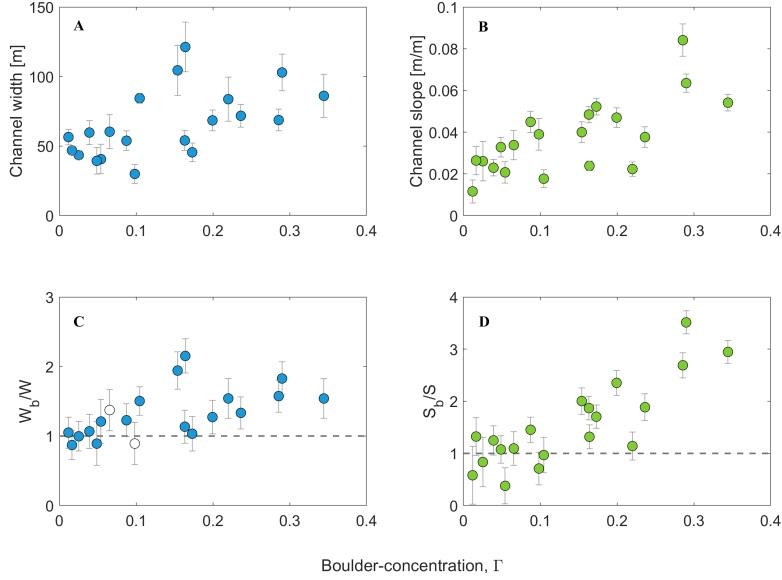
<sup>a</sup>Boulder-bed reach locations are indicated in Fig. (S1).

<sup>b</sup>BSR stands for Basin Scale Relationship, and denotes the width calculated using the relation  $W = 0.48A^{0.24}$  for channels without boulders (Fig. S3).

<sup>c</sup>GE stands for Google Earth, and denotes the average of 10 width measurements.

<sup>d</sup>Channel slope was calculated using the relation  $S = 505.4A^{-0.51}$  for channels without boulders (Fig. S3).

For information about the errors associated with calculations of  $W_b/W$  and  $S_b/S$  see supporting information.



## Theoretical framework

In this section, we develop a theoretical framework that yields steady-state analytic solutions that predict the width ratio  $W_b/W$  and the slope ratio  $S_b/S$  as functions of boulder-concentration,  $\Gamma$ . The geometrical adjustment of a boulder-bed bedrock channel is associated with two aspects of its mass balance. First, Bedrock Rivers evolve by matching their erosion rates to the applied uplift rates. Second, like alluvial rivers (e.g., Mackin, 1948), it has been argued that bedrock rivers evolve to achieve a graded state (Turowski, 2020), related to the mass balance of river sediments. Aggradation of the bed occurs if the flow is unable to carry the supplied sediments from upstream. Conversely, degradation of the bed arises when the flow’s ability to mobilize sediments is larger than the sediment supply. When the channel geometry reflects a condition where the power of the channel to mobilize sediments exactly equals upstream sediment supply, the channel is considered graded. When boulders disturb a bedrock channel, the channel responds by altering its geometry until an erosion-uplift balance and grade are met again. As is shown below, the solutions developed under the erosional balance assumption predict  $W_b/W$  as a function of  $\Gamma$ , while predictions derived from the grade assumption yield solutions involve both  $W_b/W$  and  $S_b/S$ .

### Influence of Boulders on Bedrock Erosion

The erosion rate in abrasion-dominated bedrock rivers is thought to be physically driven by the impacts of moving sediment grains during floods (e.g., Sklar and Dietrich, 1998, 2004; Turowski et al., 2007). When sediment flux increases,

more sediments are available to impact the channel bed, causing erosion and contributing to the so-called 'tools effect' (e.g., Cook et al., 2013). In contrast, when sediment flux further increases, the bed becomes shielded to impacts by sediments, consequently inhibiting erosion by the 'cover effect' (e.g., Johnson et al., 2010; Turowski and Hodge, 2017). Bedrock erosion is thus modulated by the tools effect, approximated by sediment flux per unit width  $Q_s/W$  [ $\text{kg}^1\text{s}^{-1}\text{m}^{-1}$ ], the cover effect, and the rock erodibility  $k$  [ $\text{m}^2\text{kg}^{-1}$ ], the latter determining the susceptibility of the rock to erosion and the eroded volume per sediment impact for given forcing factors. Sediment flux-dependent vertical erosion rate  $E_v$  [ $\text{ms}^{-1}$ ] is given by the product of these three terms (Sklar and Dietrich, 2004; Auel et al., 2017; Turowski, 2018)

$$E_v = k \frac{Q_s}{W} (1 - C_f) \quad (1)$$

To account for the effect of immobile boulders in Eq. (1),  $C_f$  is defined as the sediment cover due to mobile fine grains only and does not include the cover by large immobile boulders. The fine cover  $C_f$  can be calculated from a cross-sectional perspective, by dividing the width which is not covered by sediments ('uncovered width'), with the total width  $W$ . To predict steady-state channel width using Eq. (1) we need an assumption about the cover  $C_f$  at steady-state. Turowski (2018) suggested that steady-state width can be related to a length scale  $d$  [m], which indicates the distance in which a sediment particle is deflected to the side after impacting a roughness element, thereby causing bedrock wall erosion. Bedload deflected towards the sidewalls can cause wall erosion if  $d$  is larger than the cover-free channel width. In contrast, no wall erosion occurs when  $d$  is smaller than the cover-free width. At some point, the channel width adjusts such that particles almost arrive at the channel wall but do not cause erosion (Turowski, 2018, 2020). In this specific steady-state,  $d$  is equal to the uncovered width

$$C_f = \frac{W-d}{W} = 1 - \frac{d}{W}$$

Substituting (2) into (1) and solving for the width, the model predicts steady-state width to be:

$$W = \sqrt{\frac{kdQ_s}{E_v}} \quad ()$$

The sideward deflection length  $d$  is expected to vary in space and time and can be expected to depend on channel hydraulics, roughness, and sediment supply (Fuller et al., 2016a; Beer et al., 2017; Turowski, 2018, 2020b; Li et al., 2020; He et al., 2021).

We explore five potential effects of the influence of immobile boulders on steady-state channel width. For each effect, we develop an analytical expression that predicts a boulder-bed channel width  $W_{bm}$  and then use Eq. (3) to normalize it by the steady-state width of a boulder-free equivalent reach. This process leads to terms of the form  $W_{bm}/W$ , where the subscript  $b$  stands for a boulder-reach, and subscript  $m$  denotes the specific effect. When normalizing, we assume that vertical erosion in the boulder-bed channel  $E_{v,b}$  equals the erosion  $E_v$  in the

nearby boulder-free channel. Likewise, the erodibility (Eqs. 1 and 3) is assumed similar in both reaches. Consequently, both the erosion and the erodibility terms are canceled.

#### 4.1.1 The Cover Effect

Immobile boulders hinder fluvial bedrock erosion by shielding the bed (Shobe et al., 2016, 2018). However, most models that solve Eq. (1) do not consider the presence of immobile boulders with residence times larger than those of fine grains. Here, we assume a cross-section configuration with an immobile boulder in the center and a patch of fine cover that hugs one of the banks (Fig. 4). In contrast to previous works (e.g., Sklar and Dietrich, 2004), we define the riverbed fraction covered by mobile sediments as  $C_f = A_f / (A_{tot} - A_b)$ , where  $A_{tot}$  is the reach area, and  $A_f$  and  $A_b$  are the areas covered by fine sediments, and boulders, respectively. The total cover  $C_{tot}$  of the mobile sediments and immobile boulders is then written as

$$C_{tot} = 1 - (1 - C_f)(1 - \Gamma) \quad (4)$$

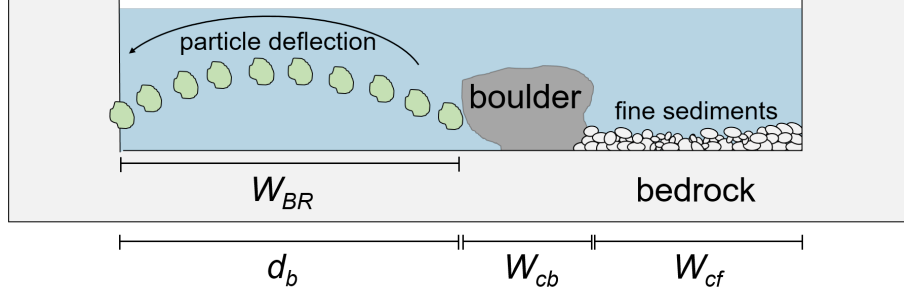
Equation (4) can be combined with the equation of vertical erosion rate (1) by replacing  $(1 - C_f)$  with  $(1 - C_{tot})$ , where both  $C_f$  and  $\Gamma$  ranges between zero and one. To illustrate this choice, when  $\Gamma$  is 0.5, half of the channel reach area is covered by boulders, and half is free to accommodate non-stationary, finer sediments. Then,  $C_f$  may be adjusted according to the remaining proportion, e.g.,  $C_f = 1$  means that the fine sediments cover the remaining bed area, half of the total reach area. In this case, the fine steady-state cover can be described using the definition for the fine sediment cover  $C_f$

$$C_f = \frac{W_{cf}}{W_b - W_{cb}} = \frac{W_b - (d_b + W_{cb})}{W_b - W_{cb}} = 1 - \frac{d_b}{W_b(1-\Gamma)} \quad (5)$$

Here,  $d_b$ , is the deflection length scale in the boulder-bed channel. Assigning Eqs. (5) and (4) into (1), solving for steady-state boulder width  $W_b$  and dividing by Eq. (3) leads to:

$$\frac{W_{bcover}}{W} = \sqrt{\frac{d_b}{d}} \quad (6)$$

Equation (6) predicts that the width ratio due to the cover mechanism by boulders is independent of boulder concentration and only depends on the square root of the ratio of channel deflection length. This independence on  $\Gamma$  derives from two opposing effects. First, vertical erosion decreases due to boulder covering the bed according to  $(1-\Gamma)$  (substitute Eq. (4) with (1)). Second, in the bed areas which are not covered, vertical erosion increases according to  $1/(1-\Gamma)$  (Eq. 5).



#### 4.1.2 The Tools Effect

In a boulder-bed channel reach, immobile boulders occupy a fraction of the total bed area, thus reducing the bed area exposed to erosion. We assume that impacting sediments acting as erosion tools can concentrate on such reduced exposed bedrock patches. Consequently, for a given cross-sectional geometry, the existence of immobile boulders increases bedload flux per unit exposed (or reduced) width. The presence of the boulders causes mobile sediments to impact on a reduced width, defined here as the effective width  $W_{eff}$ . This assumption is somewhat similar to the approach of Yager et al. (2007) and Papanicolaou et al. (2012), who assumed a reduced area for sediment transport. The resultant average effective width is the reach area free of boulders ( $A_{tot} - A_b$ ) divided by the total reach length  $L$

$$W_{eff} = W(1 - \Gamma)^\alpha \quad (7)$$

Equation (7) is derived using the relations  $A_{tot} = WL$  and  $A_b = A_{tot}\Gamma$ . The power  $\alpha$  controls the magnitude of this effect. The condition  $\alpha = 1$  applies that sediment only moves over the part of the bed without boulders, and  $\alpha = 0$  applies that sediments are also transported over the top of the boulders. Eq. (1) becomes  $E_V = k \frac{Q_s}{W_{eff}} (1 - C_f)$ . Inserting Eq. (7) into the modified (1) and solving for steady-state boulder width and dividing by (3):

$$\frac{W_{b_{tools}}}{W} = \sqrt{\frac{d_b}{d}} (1 - \Gamma)^{-\frac{(\alpha+1)}{2}} \quad (8)$$

According to Eq. (8), for  $d_b/d = 1$ , boulder-bed width increases with boulder-concentration due to the tools effect. The combination of both tools and cover effects into a single model yields

$$\frac{W_{b_{TAC}}}{W} = \sqrt{\frac{d_b}{d}} (1 - \Gamma)^{-\frac{\alpha}{2}} \quad (9)$$

In this case, the solution collapses to Eq. (6), for  $\alpha = 0$ , or indicates an increase of width with boulder-concentration for  $\alpha > 0$ .

### 4.1.3 The Multi-Channel Effect

Immobile boulders are obstacles in the channel, which are hypothesized to form small independent channels ('in-channels') between boulders as well as between boulders and the channel banks (Fig. 5). A channel reach can have two or more in-channels; the minimum set of in-channels occurs when one large boulder occupies the center of a cross-section. Consider a fluvial reach with a width  $W_b$  and a length  $L$ . There, boulders form  $n_b$  island-like columns parallel to the flow direction (Fig. 5). The total reach number of in-channels  $n_{ic}$  equals  $n_b + 1$ . Assuming cubic-shaped boulders (Fig. 5) with a diameter  $D_B$ , the number of in-channels is given by

$$n_{ic} = 1 + \frac{\Gamma W_b}{c D_B} \quad (10)$$

Here,  $c D_B$  [m] is the length of a typical pile of clustered boulders (Fig. 5), and  $c$  ( $> 1$ ) is a dimensionless parameter, assumed to equal the number of boulders constituting the boulder-island in the cross-section direction. Bedload is considered to be evenly distributed between the in-channels, such that in each of them, the average bedload flux  $\overline{Q_{s\_ic}}$  is given by

$$\overline{Q_{s\_ic}} = \frac{Q_s}{n_{ic}} = \frac{Q_s}{1 + \Gamma \frac{W_b}{c D_B}} \quad (11)$$

We assume that steady-state cover adjusts within each in-channel independently so that deflected sediments arrive precisely at the boulder or channel bank but do not cause lateral erosion. In this case, each in-channel width  $W_{ic}$  can be approximated using a form of Eq. (3)

$$W_{ic} = \sqrt{\frac{kd \overline{Q_{s\_ic}}}{E_v}} = \sqrt{\frac{kd Q_s}{E_v}} \left(1 + \Gamma \frac{W_b}{c D_B}\right)^{-0.5} \quad (12)$$

The total reach width  $W_{bMCE}$  is the sum of all in-channel widths  $W_{ic} \overline{n_{ic}}$  and the width occupied by boulders  $(\overline{n_b} - 1) c D_B$  (i.e., the number of boulders times their size)

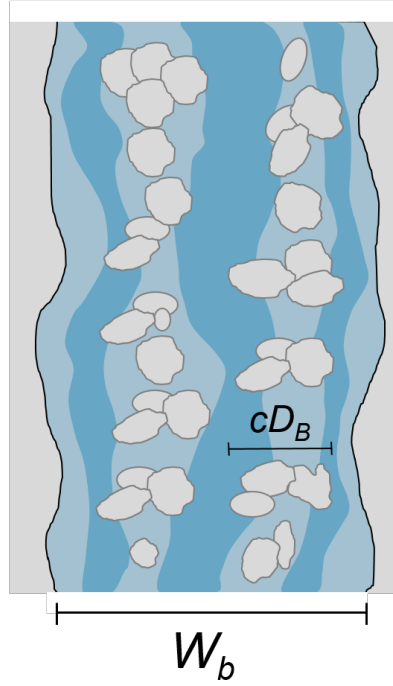
$$W_{bMCE} = W_{ic} n_{ic} + (n_{ic} - 1) c D_B \quad (13)$$

Assigning Eqs. (10)-(12) into 13, and solving for  $W_{bMCE}$ , we reach a quadratic equation with only one physically meaningful solution:

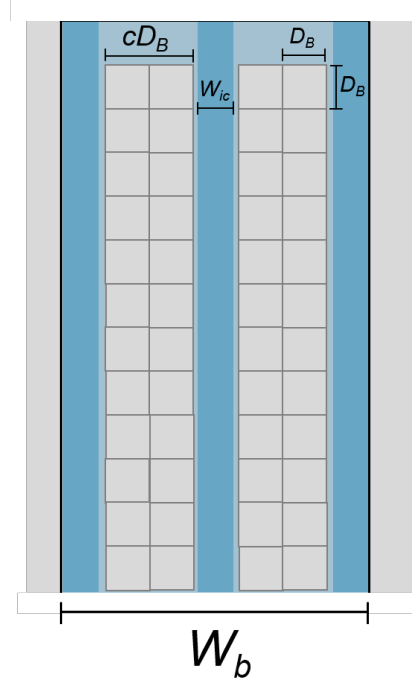
$$\frac{W_{bMCE}}{W} = \frac{1}{2(1-\Gamma)^2} \left( \frac{W\Gamma}{c D_B} + \sqrt{\left(\frac{W\Gamma}{c D_B}\right)^2 + 4(1-\Gamma)^2} \right) \quad (14)$$

where  $D_B$  is the boulder diameter. Equation (14) predicts that a boulder-channel width increases with boulder-concentration for a given  $D_B$ . Equation (14) is implicit for  $W$ , and to solve it, information on the boulder-free width,  $W$ , is needed.

## Natural settings



## Model



## Influence on Sediment Transport

The concept of grade (Gilbert, 1877; Davis, 1902; Mackin, 1948) stipulates that a channel removed from equilibrium adjusts its system variables to restore the ability to transport the same sediment supplied from upstream. A central paradigm is that channel slope adjusts to achieve grade (e.g., Mackin, 1948; Lane, 1955; Bolla Pittaluga et al., 2014; Blom et al., 2016, 2017). Various models have been developed for equilibrated channel profiles but assumed fixed channel width (e.g., Parker, 1978, 1979; Bolla Pittaluga et al., 2014; Blom et al., 2016). The graded state depends on the sediment mass balance of a river. An evolutionary mass balance representation of the sediment-bed elevation  $h_s$  is described by the Exner equation (e.g., Paola and Voller, 2005; Ancey, 2010)

$$\frac{\partial h_s}{\partial t} = -\frac{1}{\rho_s(1-p)} \frac{\partial q_s}{\partial x}, \quad (15)$$

which states that the rate of change of the sediment-bed elevation  $h_s$  with respect to time  $t$  is proportional to the divergence of sediment mass flux per unit width  $q_s$ . Here, the coordinate  $x$  denotes the streamwise direction,  $p$  is sediment porosity, and  $\rho_s$  is the sediment density. A situation where a channel is in grade implies that the derivative on the left-hand side of (15) equals zero, implying

that  $\frac{\partial q_s}{\partial x} = 0$ , and sediment flux is constant along the channel (e.g., Zhou et al., 2017).

Based on the above concept, we assume that boulder-bed channels adjust their geometry (i.e., width and slope) to accommodate a change in sediment transport due to boulder emplacement. A new equilibrium is reached when the sediment flux within the boulder-bed channel  $Q_{s,b}$  matches the sediment flux in the nearby boulder-free channel  $Q_s$ . Thus, for equilibrated boulder-bed channels, we can write

$$Q_{s,b} = Q_s \quad (16)$$

To derive the steady-state form of the adjusted boulder-bed channels, we first define a general bedload transport equation (e.g., Meyer-Peter and Müller, 1948; Fernandez Luque and Van Beek, 1976)

$$\frac{Q_s}{W} = \gamma \left( g \left( \frac{\rho_s}{\rho} - 1 \right) D^3 \right)^{0.5} (\tau^* - \tau_c^*)^{3/2} \quad (17)$$

Here,  $\tau^* = \frac{HS}{(\rho_s - \rho)D}$  is the Shields number,  $H$  is flow depth [m],  $\tau_c^*$  is the critical Shields stress for bedload incipient motion,  $D$  [m] is bedload grain size,  $g$  [9.81 ms<sup>-2</sup>] is the acceleration due to gravity, and  $\gamma$  is a non-dimensional constant larger than one (Fernandez Luque and Van Beek, 1976; Wong and Parker, 2006). Equation (17) can be replaced by a discharge-based equation for sediment transport (Rickenmann, 2001), which takes the form of (e.g., Turowski, 2021)

$$\frac{Q_s}{W^q} = K_{BL} Q^m S^n \quad (18)$$

Here,  $Q$  is water discharge, and  $K_{BL}$  is a constant describing transport efficiency. The exponent  $m$  typically takes values between 1 and 4 (Barry et al., 2004), while  $n$  ranges between 1.5 to 2 (Rickenmann, 2001). The exponent  $q$  sets the dependence of bedload transport on channel width and is often assumed to be equal to zero (e.g., Rickenmann, 2001). However, given the unsteady nature of bedload transport and along-stream variations in channel width (Cook et al., 2020), the parameter  $q$  may differ from zero. Analytically derived end-member approximations have been discussed by Turowski (2021), which give values for  $q$  of zero, 0.1, or 2.5.

The influence of boulders on sediment transport can be considered via the boulder effects on the various parameters in equations (17) and (18) (Shobe et al., 2021). A reduction in the effective shear-stress ( $\tau^* - \tau_c^*$ ) is associated with two different hypothesized effects (Schneider et al., 2015a): (i) a reduction in  $\tau^*$  due to fluid friction forces (e.g., Canovaro et al., 2007; Yager et al., 2007; Nitsche et al., 2011) and (ii) an increase in the threshold of motion  $\tau_c^*$  with channel slope (Lamb et al., 2008; Prancevic and Lamb, 2015), which is thought to increase with boulder-concentration (Nitsche et al., 2011; Thaler and Covington, 2016; Shobe et al., 2020). Similarly, there might be a reduction in the bedload transport efficiency for a given shear-stress (Rickenmann, 2001; Nitsche et al., 2011) due to particles either taking longer pathways or being transported slower due

to boulder-influenced hydrodynamic effects (Papanicolaou et al., 2018). Based on these effects, we establish two theoretical models that predict the relation between the width and slope ratios. We begin in section 4.2.1 with analytical solutions assuming a reduction in the coefficient of transport efficiency and continue in section 4.2.2 by considering a reduction in the Shields-number due to fluid friction forces on boulders. Additional potential effects of an increase in the threshold of motion  $\tau_c^*$  due to boulders, and a reduction in the energy slope for bedload transport (e.g., Chiari et al., 2010) are acknowledged, but are not treated in this paper.

#### 4.2.1 Reduction in Bedload Transport Efficiency

A boulder placed into a steady-state channel is expected to change the river’s ability to carry bedload sediments. A reduction in the transport efficiency is expected because, during a transport event, sediments can (i) be deposited in the wake-zones of boulders due to flow reversals (e.g., Papanicolaou and Tsakiris, 2017; Papanicolaou et al., 2018), thus delaying their overall movement downstream, (ii) lose momentum due to direct encounters with boulder-influenced zones, and (iii) take longer pathways relative to a similar boulder-free channel (e.g., Seizilles et al., 2014). The new condition adjusts the channel geometry to a new state where transport capacity equals the sediment supply. This can be achieved via changing slope, width, or both (Eq. 18). Rickenmann (2001) showed for flume and field bedload transport data that transport efficiency decreases with relative roughness (ratio of flow depth to grain size) by up to five orders of magnitudes. Nitsche et al. (2011) studied flow and bedload transport characteristics in 13 Swiss streams. They showed that fractional transport efficiency  $K'_{BL}/K_{BL}$ , where  $K'_{BL}$  is the reduced transport efficiency coefficient due to roughness, decreases with boulder-concentration. Using digitization of their bedload data (their Fig. 8e), we fitted the relation between  $K'_{BL}/K_{BL}$  and  $\Gamma$  with:

$$\frac{K'_{BL}}{K_{BL}} = \frac{1}{1+(\theta-1)\Gamma^\nu} \quad (19)$$

Equation (19) is an empirical function with a factor  $\theta$  and a power  $\nu$ . Substituting Eq. (18) into (16) leads to:

$$K'_{BL} Q^m W_{b_{STE}}^q S_{b_{STE}}^n = K_{BL} Q^m W^q S^n \quad (20)$$

And solving for the slope ratio using (19)

$$\frac{S_{b_{STE}}}{S} = \left( \frac{W_{b_{STE}}}{W} \right)^{-q/n} (1 + (\theta - 1)\Gamma^\nu)^{1/n} \quad (21)$$

Here,  $S_{b_{STE}}/S$  and  $W_{b_{STE}}/W$  are dependent variables, whereas  $\Gamma$  is independent and  $q$ ,  $n$ ,  $\theta$ , and  $\nu$  are empirical parameters. Closing equation (21) requires that the width ratio is substituted with either one of the models derived in section 3.1 or supplied with field data.

## 4.2. The effect of Shear-Stress Partitioning

The total shear stress acting on a channel boundary is commonly used as a first-order parameter for prediction of bedload fluxes (e.g., eq. 18; Einstein, 1950; Fernandez Luque and Van Beek, 1976; Rickenmann, 2001). However, many bedload transport equations were derived based on flume experiments, where the geometry is simplified and roughness is considered to be steady. Natural bedrock channels often exhibit bedforms and large grains, which act as obstacles to the flow, altering water velocity gradients and associated shear stresses. Mainly, roughness elements bear a fraction of the total available shear-stress, thus decreasing the available shear stress for entrainment of bedload. Einstein and Banks (1950) suggested that the total resistance to roughness elements equals the sum of the resistance of each of the individual components. This partitioning approach for transport predictions was further developed for immobile boulders (Yager et al., 2007). We adopt this approach to predict channel width and slope in boulder-bed channels, acknowledging that boulders are roughness elements. Following Yager et al. (2007), we partition the channel bed into a fine-grained, mobile bedload fraction (denoted by the subscript  $m$ ) with a characteristic grain size  $D$  and immobile boulders with a diameter of  $D_B$ . Shear-stresses are not additive, i.e., the total shear-stress does not equal the sum of all stresses. Instead, forces are additive; hence we can assume a fluid force balance between the driving forces  $F_{tot}$  and the resisting forces  $F_d$  and  $F_m$ .

$$\tau A_{tot} = \tau_d A_d + \tau_m A_m \quad (22)$$

Here,  $F_m = \tau_m A_m$  is the resisting force due to the roughness of the channel bed without boulders, which encompasses both skin friction and drag (Dey, 2014),  $F_d = \tau_d A_d$  is the resisting force due to drag on boulders, and  $A_{tot}$ ,  $A_d$  and  $A_m$  are the channel areas upon which the forces are applied, respectively. The skin friction component due to boulders  $F_s$  is assumed to be negligible. To facilitate area calculations, we can divide Eq. (22) by the total reach area  $A_{tot}$  to obtain

$$\tau = \tau_d \frac{A_d}{A_{tot}} + \tau_m \frac{A_m}{A_{tot}} \quad (23)$$

In a large flood, the entire bed is submerged, and the mobile area  $A_m$  upon which drag applies is proportional to the overhead projection area without boulders, i.e.,  $A_m/A_{tot} = (1-\Gamma)$ . However, boulders extend into the flow; thus, drag forces act mostly on their upstream sides and  $A_d = nD_B^2$ , with  $n$  being the number of boulders in the reach. Using the definitions for boulder-concentration  $\Gamma = nD_B^2/WL$  and for the reach area  $A_{tot} = WL$ , we introduce  $A_d/A_{tot} = \Gamma$ . Thus, (23) can be rewritten as:

$$\tau = \tau_d \Gamma + \tau_m (1 - \Gamma) \quad (24)$$

Considering that boulders reduce the total shear stress, we aim to find an expression for the reduced shear stress,  $\tau_m/\tau$ , which we assume is responsible for fine sediment transport. First, the fractional boulder-drag stress  $\tau_d/\tau$  can be evaluated using a general empirical log-linear model based on experimental results from Canovaro et al. (2007):

$$\frac{\tau_d}{\tau} = \beta\Gamma \left[ 1 - \ln \left( \frac{\Gamma}{\Gamma_{max}} \right) \right]; \quad 0 < \Gamma \leq e\Gamma_{max}$$

Here,  $\Gamma_{max}$  is the boulder-concentration for which  $d/\lambda$  is maximal,  $\beta$  is a scaling factor, and  $e$  is the natural base logarithm constant. The maximal  $d/\lambda$  value can be derived by applying  $\Gamma = \Gamma_{max}$ , which in that case  $(d/\lambda)_{max} = \Gamma_{max}$ . The random-boulder setting experiments of Canovaro et al. (2007) show that  $\Gamma_{max}$  is relatively limited and ranges from  $\sim 0.2$  to  $0.4$ . The condition  $\Gamma \leq e\Gamma_{max}$  verifies that  $d/\lambda$  do not yield negative, unrealistic values. Substituting Eqs. (2) and (25) into (22) and solving for  $m/\lambda$

$$\frac{\tau_m}{\tau} = \frac{1}{1-\Gamma} \left[ 1 - \Gamma \left[ 1 - \ln \left( \frac{\Gamma}{\Gamma_{max}} \right) \right] \right]$$

If only the effect of shear stress partitioning is considered, then the combination of (16) and (17) implies

$$W_{bSSP} \tau_m^{*3/2} \sim W \tau^{*3/2}$$

Rearranging (27) and solving for  $W_b/W$  using the definition for the Shield-stress  $\tau^* = \frac{\tau}{gD(\rho_s - \rho)}$  and  $\tau_m^* = \frac{\tau_m}{gD(\rho_s - \rho)}$  and Eq. (26)

$$\frac{W_{bSSP}}{W} = \left( \frac{\tau_m}{\tau} \right)^{-3/2} = \left[ \frac{1}{1-\Gamma} \left( 1 - \Gamma \left[ 1 - \ln \left( \frac{\Gamma}{\Gamma_{max}} \right) \right] \right) \right]^{-3/2} \quad (28)$$

The effect of shear-stress partitioning can alternatively be expressed in terms of the slope ratio (Appendix A)

$$\frac{S_{bSSP}}{S} = \left( \frac{1}{1-\Gamma} \left[ 1 - \Gamma \left[ 1 - \ln \left( \frac{\Gamma}{\Gamma_{max}} \right) \right] \right] \right)^{\frac{\delta-0.5}{\delta+0.5}} \quad (29)$$

Where  $\delta$  is an exponent relating water velocity to the hydraulic radius  $R_h$  and equals  $1/2$  for a Darcy-Weisbach relation or  $2/3$  for a Manning-Strickler relation. For  $\delta$  equals  $1/2$ , the right-hand side of (29) equals one, and the boulder-bed channel slope  $S_b$  equals the boulder-free channel slope, whereas when  $\delta$  equals  $2/3$ , the slope ratio  $S_b/S$  depends on the expression on the right-hand side of (29) to the power of  $1/7$ . With such a low exponent, the effect of shear-stress partitioning on the slope ratio is expected to be small and is not likely to reproduce the data.

**Table 2:** Models performances of the width and slope ratios.

Assumption	Mechanism	Prediction	<sup>a</sup> Parameters	<sup>b</sup> RMSE
Erosional balance: bedrock erosion matches between boulder-bed and boulder-free channels	Cover	$\frac{W_{b_{cover}}}{W} = \sqrt{\frac{d_b}{d}}$	$d_b = d$	
	Tools	$\frac{W_{b_{tools}}}{W} = \sqrt{\frac{d_b}{d}} (1 - \Gamma)^{-\frac{(\alpha+1)}{2}}$	$= 0$ $= 1$	
	Tools and Cover	$\frac{W_{b_{TAC}}}{W} = \sqrt{\frac{d_b}{d}} (1 - \Gamma)^{-\frac{\alpha}{2}}$	$= 0$ $= 1$	
	Multi- channel Effect	$\frac{W_{b_{MCE}}}{W} = \frac{1}{2(1-\Gamma)^2} \left( \frac{W\Gamma}{c} + \sqrt{\left( \frac{W\Gamma}{cD_B} \right)^2 + 4(1-\Gamma)^2} \right)$	$c =$	
Grade: sediment flux between boulder-bed and boulder-free channels equals	Reduction in Sediment Transport Efficiency	$\frac{S_{b_{STE}}}{S} = \left( \frac{W_b}{W} \right)^{-q/n} (1 + (\theta - 1)\Gamma^\nu)^{1/n}$	$q = 0$	
	Shear-stress Partitioning	$\frac{W_{b_{SSP}}}{W} = \left[ \frac{1}{1-\Gamma} (1 - \Gamma \left[ 1 - \frac{\Gamma}{\Gamma_{max}} \right]^{0.30}) \right]^{-3/2}$ $\frac{S_{b_{SSP}}}{S} = \left( \frac{1}{1-\Gamma} [1 - \Gamma \left[ 1 - \frac{\Gamma}{\Gamma_{max}} \right]^{0.30}] \right)^{\frac{\delta-0.5}{\delta+0.5}}$	$q = 0.1$ $q = 1$ $= 1.38$ $= 1.38$	

<sup>a</sup>The parameter values used to examine the models against the Liwu data.

<sup>b</sup>Root Mean Square Error calculated between the Liwu data and the examined model.

## Model Evaluation using the Liwu River Data

The mechanisms introduced in Section 4 yield five equations for the width and two for the slope ratio (Table 2). These can be tested against the Liwu River data (Fig. 3). Each model contains various parameters, some of which could not be independently constrained. Due to the scatter in the width ratio versus boulder-concentration (Fig. 3C), we do not expect a single set of parameters to predict the entire width ratio dataset. Moreover, plotting a single model with specific parameter values requires calibration against field data, which will bias the model towards good performance. Instead, we analyze slope and width ratio sensitivity to parameter changes within the different models by plotting model results for different parameter scenarios while holding other parameters constant.

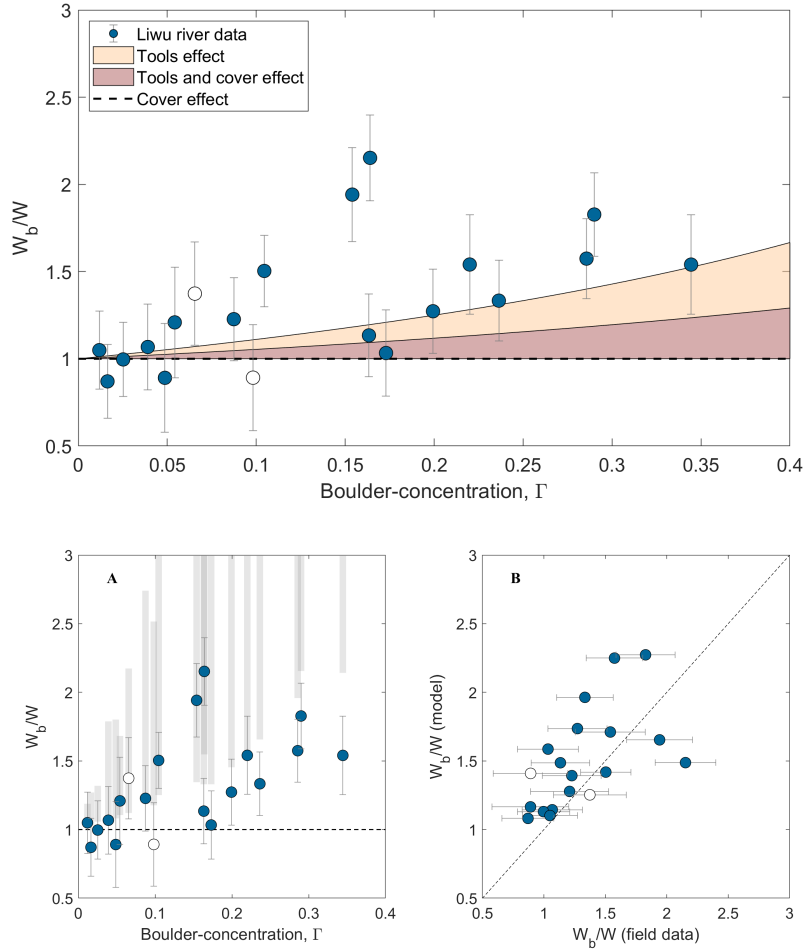
### 5.1 The Tools, Cover, 'Tools and Cover,' and Multi-Channel Effect Models

The cover (Eq. 6), the tools (Eq. 8), and the combined 'tools and cover' (Eq. 9) effects can be solved explicitly and can therefore be directly compared to the field data. We first note that the cover model is independent of boulder concentration (Fig. 6). Its prediction does not follow the trend observed in the field data and is equivalent to a case where  $W_b = W$ . This trivial model yields an RMSE value of 0.48, which forms a benchmark error to which the various width models are compared (Table 2).

The tools and the 'tools and cover' effects contain one free parameter,  $\alpha$ , which could vary between zero and one, and  $d_b/d = 1$  is assumed throughout the analysis. In the case of  $\alpha = 0$ , both models yield the trivial result of  $W_b = W$ . Therefore, we turn to present the results of the two models using  $\alpha = 1$ . The tools effect predicts an increase in the width ratio with boulder-concentration (Fig. 6), with a model-data RMSE of 0.40 (Table 2). Although a lower RMSE value than the trivial model, the tools effect underpredicts most of the data. The 'tools and cover' model predicts an increase in the width ratio similar to the tools model. Still, it predicts an even smaller exponent and underpredicts the field data, yielding an RMSE value of 0.40.

The multi-channel effect, Eq. (14), is implicit for the boulder-free width  $W$ , which also appears on the right-hand side of the equation. Therefore, to compare the model to data, we assign the measured values of boulder-free width  $W$  (using the Google-Earth derived channel width; see Fig. S2), mean boulder diameter  $D_B$ , and boulder-concentration for each data point. The parameter  $c$  can be interpreted as the number of boulders constituting a boulder pile along the

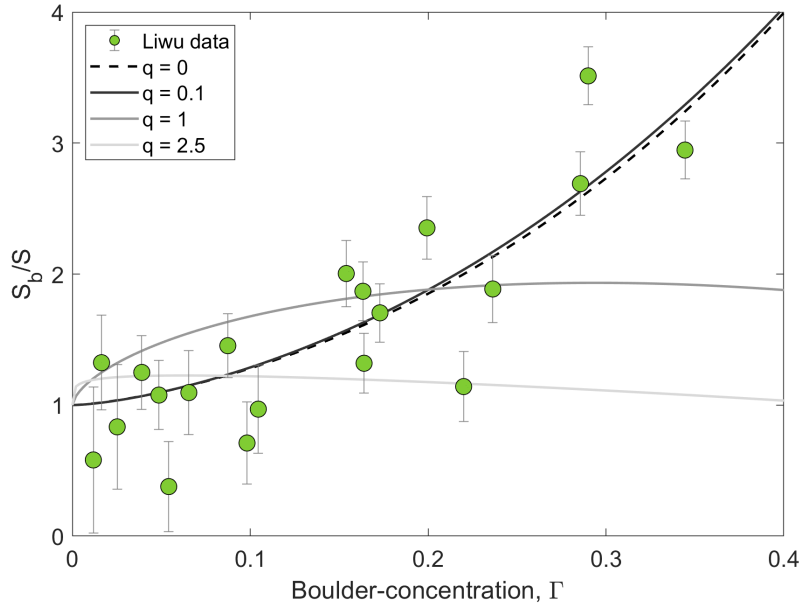
cross-section (Fig. 5). Here, to represent the uncertainty in  $c$ , we assume that it takes values between 1 and 4. The multi-channel model plots relatively close to the field data (Fig. 7A). Considering the error on  $W_b/W$  and the uncertainty in  $c$ , the model accounts for 75% of the Liwu width ratio data. The RMSE between the field and best-fit model width ratios is 0.51, which is larger than the prediction for  $W_b = W$ .



## 5.2 Reduction in Sediment Transport Efficiency

The reduction of sediment transport efficiency model, equation (21), combines both the width and slope ratios and therefore requires a second equation or independent data to close the system. Furthermore, to solve equation (21), the parameters  $q$ ,  $n$ ,  $\beta$ , and  $\gamma$  need to be constrained. The parameter  $q$  was shown to take end-member values of 0, 0.1, 1, and 5/2 (Section 2.1). We study the

behavior of  $q$  on the model since its appearance in Eq. (21) implies a covariant effect of channel width and channel slope. For each  $q$  value explored, we iterated and chose random values of the remaining unknown parameters:  $n$ ,  $\beta$ , and  $\gamma$  from a specified range of values and selected those that minimized the RMSE value between the model output and the Liwu data. Using the tools model to replace  $W_b/W$  and  $\beta = 1$ , when  $q$  is low (i.e., equals zero or 0.1), the model captures the increase in  $S_b/S$  with  $\Gamma$  (Fig. 8). In contrast, for larger values of  $q$ , the model deviates significantly from the data. The model performs best (lowest RMSE) when  $q$  is close to or set to zero (Table 2), which corresponds to a case where the slope ratio  $S_b/S$  is independent of the width ratio  $W_b/W$ .

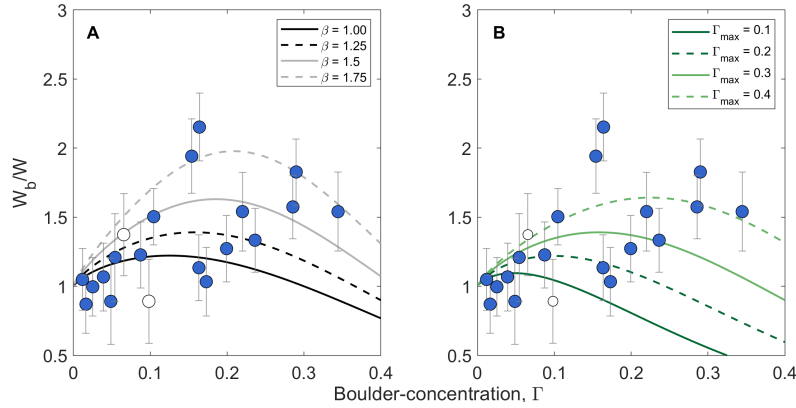


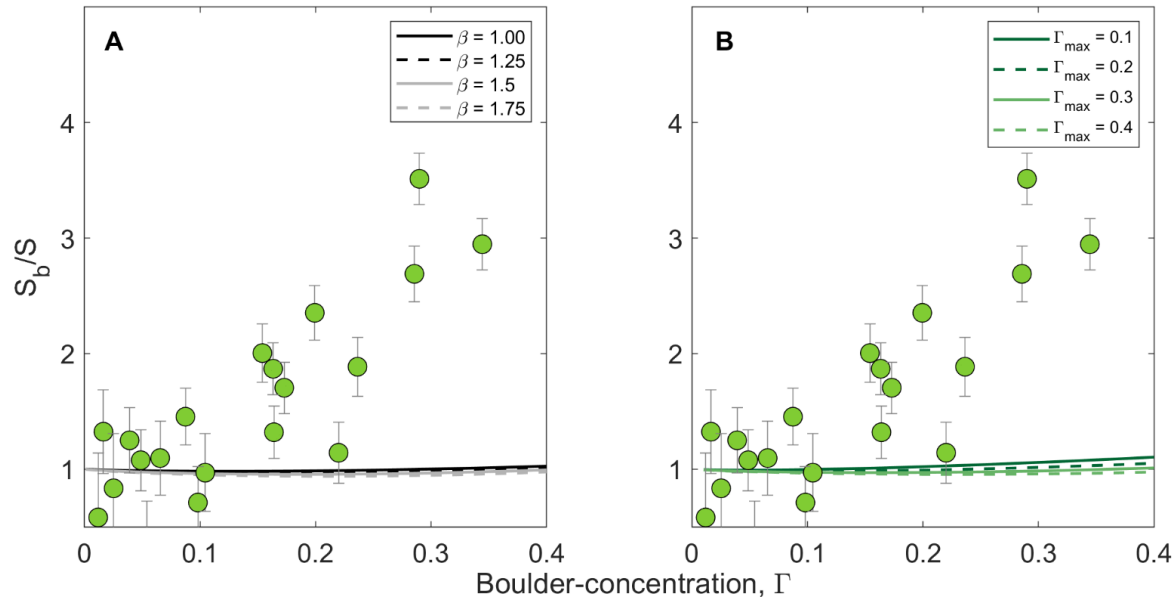
### 5.3 The Effect of Shear-stress Partitioning

Here we aim to examine whether the shear-stress partitioning model can independently explain the Liwu River width and slope ratios. To test the model, we changed either  $\beta$  or  $\Gamma_{max}$ , while treating the other as a constant (see below). The parameter  $\beta$  defines how fast the normalized drag stress increases with increasing  $\Gamma$  (Eq. 25). In contrast,  $\Gamma_{max}$  is the boulder concentration where the normalized drag stress reaches its maximum. We note that both parameters are only constrained from flume experiments (Canovaro et al., 2007). Digitizing Canovaro et al.'s (2007) data sets,  $\beta$  ranges between 1.8 and 4.2, while  $\Gamma_{max}$  varies from 0.18 to 0.37. We tested Eq. (28) by first plotting model predictions using a constant  $\Gamma_{max} = 0.3$  while exploring a range of  $\beta$  values that fit the width ratio data. Then,  $\beta = 1.25$  was held constant while  $\Gamma_{max}$  values were varied to study their role in controlling model behavior.

Exploring the model, we find that it predicts a non-monotonic trend. At small boulder concentrations, the width ratio is predicted to increase, then it reaches a maximum, after which it predicts a decrease in width ratio with increasing boulder concentration (Fig. 10). For a given  $\Gamma_{max}$ , larger  $\beta$  shifts the width ratio maxima and magnitude towards larger  $\Gamma$  values and larger  $W_b/W$  values, respectively (Fig. A). A similar behavior is observed when increasing  $\Gamma_{max}$  (Fig.9B). A model with  $\beta = 1.0$  captures 60% of the width ratio data within one STD error, so does  $\beta = 1.25$ . To test whether the data set can be described by a non-monotonic model, we evaluated Spearman’s rank correlation coefficient between the width ratio and boulder-concentration. A calculated value of 0.65 implies that the two variables are positively correlated (for comparison, the rank correlation coefficient between the slope ratio and  $\Gamma$  is 0.76). However, a non-monotonic relationship cannot be ruled out.

Considering the effect of the shear stress partitioning on the slope ratio, in section 3.2.2, we showed that the slope ratio depends on boulder concentration to a maximum power of  $1/7$ . Regardless of the choice of the other free parameters, this produces only a weak dependency between the slope ratio and boulder concentration, which makes the shear stress partitioning model inadequate to describe the Liwu slope ratio data (Fig. 10).





## Discussion

### Reviewing the Assumptions of Steady-States

In our theoretical framework, we have assumed steady-state and tested the resulting equations using field data from the Liwu River. Among the examined models, some have produced higher goodness-of-fit values (e.g., the reduction of transport efficiency effect), while others showed a certain degree of incompatibility compared to the data (Section 4; Table 2), thus requiring an assessment of the applicability of the steady-state assumptions.

#### *Steady-State in the Erosional Balance Assumption*

Under the steady-state assumption in the erosional balance, we assume that (i) neighboring boulder-bed and boulder-free reach incise at the same rate. A substantial difference in incision rates between two adjacent channel reaches would promote a knickpoint between the two reaches. We have not observed any such prominent knickpoint at any of the 20 studied sites. (ii) The channel width is at steady-state with respect to erosion rate and fine cover (Turowski, 2018). This assumption is valid if boulders are present at the same reach-averaged concentration at a particular location for a sufficiently long time. In numerous reaches that we examined, there is direct evidence for a continuous supply of large boulders (Text S3). Hillslopes nearby boulder-bed channels often exhibit scars typical of landslides and rockfalls. However, whether those boulders were delivered to the Liwu tributaries recently or if they were placed a long time

ago requires further research. Field evidence from other tectonically active sites demonstrates that boulders may last in rivers for periods of tens of thousands of years (Haviv, 2007; Huber et al., 2020). However, a steady-state width configuration is also dependent on how fast the channel widens in response to boulder input. Direct bedrock erosion measurements from the Liwu river reveal that locally, lateral bank erosion can be as significant at tens of centimeters in a single flood season (Hartshorn et al., 2002; Turowski et al., 2008). Hence, channel widening probably occurs much faster in the Liwu River than elsewhere. Ultimately, boulder-bed channel width in the Liwu river may be at a steady-state with respect to uplift, sediment supply, and discharge, but whether width has completely adjusted to boulder input requires further investigations concerning the durability of boulders once they arrive into the river domain. It is also possible that we have not considered different mechanisms responsible for the width anomaly in the Liwu River.

#### *Steady-State in the Grade Assumption*

Under the assumption of a grade steady state, we have assumed that sediment-flux in the boulder-bed and boulder-free reaches are the same. This assumption does not require a continuous supply of boulders into the channel but rather a fast response of the river to change the ability to transport sediment with the same efficiency due to boulder-concentration. Specifically, according to Eq. (15), the 'grade' assumption requires that sediment-bed elevation  $h_s$  above the bedrock is steady in the long term. Thus, for a channel that has been recently supplied with large boulders, how rapidly can a river restore its sediment transport capacity? We demonstrated that grade conditions could be achieved by adjusting the sediment thickness to form a new channel slope. The rate at which new sediment bed slope forms depends on various hydrological and morphological parameters, such as water discharge, shear stress, and the grain size of the mobile sediment (e.g., Barry et al., 2004). The Liwu river may be a locality in which large variability in water discharge (Lague et al., 2005) and magnitude are expected to promote more sediment transport events in a given flood season (Hartshorn et al., 2002; Dadson et al., 2003). For example, observations from the Liwu River show that the river can remove sediment a few meters in depth following a significant typhoon event (Lague, 2010). Even if boulders disappear quickly once arriving in the fluvial system, the timescale of bedload entrainment and deposition to form a new sediment slope in general and grade conditions, in particular, may correspond to a single flood (Turowski, 2020). Field evidence from various bedrock channels supports recognizing an equilibrium, or 'grade,' in many bedrock river environments (Phillips and Jerolmack, 2016), reinforcing the plausible assumption that the Liwu river is at an approximate sediment transport steady-state, or in grade, at nearly all times.

## **Evaluation of the Theoretical Models**

Under the two steady-state assumptions described in sections .1 and .2, we formalized five mechanisms presumably underlying the observations of both widen-

ing and steepening of boulder-bed channels (Table 2). Below, we examine and discuss the performance of the models to describe the Liwu data channel width and slope predictions using the erosional balance and grade-based mechanisms

Five models have been considered for testing the width ratio,  $W_b/W$ : the cover, the tools, the 'tools and cover,' the multi-channel effect, and the shear-stress partitioning effect. The first three models are dependent on the ratio of the square root of boulder-bed to boulder-free deflection lengths (Eqs. 6, 8, and 9), which we assumed to be one, i.e.,  $d_b = d$ . The deflection length likely depends on grain size, hydraulic parameters (Turowski, 2020), the contact angle of the boulder with the mobile particle (Fuller et al., 2016; Beer et al., 2017; Li et al., 2020), bedload path relative to the location of a roughness zone (He et al., 2021), and fluid shear stress (Li et al., 2020; Turowski, 2020). The influence of boulder concentration on sediment deflection is currently unknown, but a positive correlation may account for channel widening for the above-discussed models beyond the predictions with  $d_b = d$ .

The cover model predicts that  $W_b/W$  equals  $\sqrt{\frac{d_b}{d}}$ , meaning that as long as  $d_b = d$ , (I) the width ratio does not independently depend on  $\Gamma$ , and (II) there is no boulder-bed widening with respect to a boulder-free reach. Considering the above, although our theoretical framework of the cover effect does not reproduce the Liwu width ratio data, future advances in our understanding of the relation between deflection length and roughness elements could lead to a modified cover model for channel width that depends on  $\Gamma$  as has been hypothesized for slope (Shobe et al., 2021).

The tools (Eq. 8) and the 'tools and cover' (Eq. 9) models predict an increase in the width ratio with boulder-concentration (Fig. 6). The essential difference between the two models is in the exponent, which depends on the parameter  $\beta$ , describing whether bedload particles are routed above boulders ( $\beta = 0$ ) or not ( $\beta = 1$ ). At the process scale, large boulders protruding into the flow are thought to encourage sediment deposition around them (e.g., Papanicolaou and Kramer, 2006; Tsakiris et al., 2014; Polvi, 2021), which may lead to substantially different protrusion, causing bedload transport to alter significantly (Yager et al., 2007). We thus hypothesize that boulder protrusion and hydraulic behavior near boulders have an essential role in controlling  $W_b/W$ .

The multi-channel effect (Eq. 14) predicts an increase in the width ratio with boulder concentration (Fig. 7). For a given boulder-bed channel, the model plots relatively close to the data but commonly overpredicts it, especially for large boulder-concentration values. Given the overall over-prediction of the data and the relatively large RMSE value, we propose that the model with its current assumptions is unsuitable for boulder-bed channels in the Liwu River. We envision three major potential causes for the model-data deviations.

The model was derived using three primary assumptions: (I) the channel reach follows a specific geometry, including boulder arrangement (Fig. 5), (II) sed-

iments are redistributed evenly between the in-channels, and (III) the overall boulder-bed channel width independently reflects a steady-state configuration for every in-channel. The Liwu boulder-bed channel reaches, however, exhibit a wide range of boulder sizes and inner-reach distributions. Furthermore, at bankfull flows, when the entire bed is submerged, sediments are expected to follow paths set by the flow hydrodynamics—rather than the configuration of boulders—and not be evenly distributed. We believe that some of the scatter of the data concerning model predictions are due to such discrepancies. To better capture the width ratio variability, specific treatments of boulder distributions and sediment paths can be considered in future studies

The effect of shear-stress partitioning shows a humped relationship between width ratio and  $\Gamma$ , which can be explained by the non-monotonic log-linear model Eq. (25) used to derive the model. Although the effect captures 60% of the data within the errors, we emphasize two reasons for the model’s inadequacy of the Liwu data. First, a simpler, linear model could also account for that fraction captured by the non-monotonic model. Second, the parameters  $\Gamma$  and  $\Gamma_{max}$  need to be different between the different reaches, but independent constraints on their values are missing. As a result, the shear-stress partitioning model cannot predict well the width ratio. While the physical interpretation of  $\Gamma$  is unclear, we cannot evaluate the extent to which this parameter should vary among the examined reaches. Differences between channel reaches could emerge from contrasts in the boulder size distributions and the streamwise and cross-sectional location distributions.

Although the tools and shear-stress partitioning models statistically performed best overall (Table 2), the role of multi-channels in shaping boulder-bed channel width cannot be ruled out. Furthermore, additional investigations are awaiting to unravel the role of cover in the relationship between width and boulder presence (e.g., Shobe et al., 2020). However, the overall inability of the models to account for the width anomaly in the Liwu River, and the long timescale of width adjustment implied from the scatter in our data all drive us to suspect that different reaches have adjusted to boulder input to various degrees.

Two models have been considered for testing the slope ratio,  $S_b/S$ : reduction in transport efficiency and shear-stress partitioning. Both were developed under the assumption of grade. We first note that the shear-stress partitioning effect cannot explain the slope ratio increase in the Liwu River (Fig. 10). Thus, this model can be ruled out in explaining the increase in width ratio with boulder-concentration. The prediction of the reduction in transport efficiency model could explain the trend observed in the data (Fig. 8) yet requires calibration of four parameters. Although, according to this model, in the general case, the slope ratio is a function of the width ratio, we find that the best-fit parameters are those that make the slope ratio independent of the width ratio. This outcome points to a steepening effect that relies solely on sediment entrainment and deposition to form a steeper bed and can occur very fast, probably within one or a few floods. This mechanism differs from the one developed by Shobe et

al. (2020), which relied on bedrock erosion to accomplish the slope change, and would therefore have a much longer adjustment timescale. The inferred independence of the slope ratio and the width ratio, manifested by the small  $q$  (power of the width ratio), may be a consequence of the substantial difference in the adjustment timescales of bedrock width and sediment-bed slope (Turowski, 2020). In other localities with much softer and erodible banks (e.g., Cook et al., 2014), the covariation of slope and width are hypothesized to be more significant. Whereas standard models commonly assume that  $q$  is either zero or one, it is also possible that the dependence of sediment flux on channel width is diminished in the long term, thus constraining  $q$  to be close to zero (Rickenmann, 2001). Further research on the value  $q$  for different timescales of sediment transport is needed. Given the good fit and the general agreement of the model with the data, we attribute most of the steepening of the boulder-bed channel reaches to a necessity to mobilize the upstream sediment supply despite the presence of boulders that inhibit sediment transport efficiency.

The reduction in transport efficiency model further predicts a monotonic steepening effect with increasing boulder concentration. However, with increasing boulder concentration, we expect channel slope response to potentially reduce as the channel self-organizes a new bed largely composed of boulders such that boulders are no longer significant roughness elements on the bed. This situation is equivalent to the role of boulder spacing, shown by flume experiments, to strongly influence grade conditions (McKie et al., 2021). Each boulder generates a unique zone susceptible to flow reversals and enhanced turbulence (Papanicolaou and Tsakiris, 2017). However, when the spacing is small, the different boulder-influenced zones interact, causing an overall reduction in the total influence zone. Our developed equation does not show this behavior because of the assumption that the transport efficiency reduces monotonically for the entire range of  $\Gamma$  (Eq. 19).

## Causality Relations between Boulder Concentration and Channel Width

The models proposed to explain the observed relation between boulder concentration and the width ratio assume that channel width adjusts (and is, therefore, the dependent variable) to boulder concentration. Notwithstanding, the causality between the two variables can also be presented inversely. Here we pose a hypothesis for a potential dependence of boulder-concentration on channel width. Consider a case in which boulders have an equal probability of arriving at a specific location within the river and assume an initial natural variability in channel width along the river. In wider reaches, the fluid shear-stress deriving both bedload transport, which is responsible for boulder abrasion (Wilson et al., 2013) and boulder transportation, is smaller relative to a narrow channel with otherwise the same parameters. Since bedload transport depends on discharge and erosion depends on bedload, boulders will both abrade and be transported quicker in narrower channels. In such a case, observations would be of a positive

scaling of channel width with boulder concentration. However, we specify three reasons why such a case is probably not valid for the Liwu River. First, we do not have direct evidence for initial width variability. Second, an initial spatial variability in channel width between neighborhood reaches is less likely because our paired approach of width normalization should also account for lithological and bank properties.

The unknown directionality between boulder-concentration and the channel width is a '*chicken or egg?*' problem, where cause and causality between the two variables are potentially bi-directional. Ultimately, we speculate that once boulders arrive into the channel, the effects outlined above interact to form a new steady-state width configuration (Turowski, 2018). Nearby failure events can produce new boulders, which in turn contribute to the adjustment of channel width.

## Conclusions

We studied the controls of large immobile boulders on channel width and slope in bedrock channels. Our data from the Liwu River, Taiwan, show that sediment-bed slope and bedrock width increase in response to higher concentrations of boulders after width and slope are normalized for variations due to drainage area. We invoked rock and sediment mass balance principles to explore possible mechanisms responsible for the observed width and slope increase with boulder concentration. We combined them in a theoretical framework for fluvial bedrock erosion and sediment transport. The theoretical framework yields analytic predictions for the width and slope ratios as a function of boulder concentration.

Under the first principle of rock mass balance, we assumed that boulder-bed and boulder-free reaches incise into bedrock at the same rate. We expanded this assumption by considering three effects that boulders impose on the process of bedrock erosion: the cover, the tools, and the multi-channel effect. These models yielded solutions to the width ratio. Under the second principle, we assumed that bedload flux in adjacent boulder-bed and boulder-free reaches is identical under equilibrated grade conditions. Here, two underlying mechanisms were examined for the effect of boulders on bedload transport: a reduction in the efficiency of sediment mobilization and a reduction in the shear stress responsible for sediment mobilization. Both mechanisms yielded solutions for the slope ratios, while the second mechanism provided an independent solution to the width ratio.

The width ratio trend was best captured by the tools effect, yet this model underpredicted most of the data. The shear-stress partitioning model can account for a fraction of the width data, but requires knowledge on its numerous parameters, which are not constrained. Under the boulder cover effect, width is insensitive to boulder concentration. Still, an emerging relationship between sediment deflection and the existence of boulders is hypothesized to yield a link

between width and boulder-concentration due to a boulder cover effect. The multi-channel effect demonstrated an increase of width but predicted larger width values than mostly seen in the Liwu data. We conclude that the scatter in the data points out to a long timescale adjustment of channel width, and different reaches have adjusted to different extents.

The slope ratio was best captured by the effect of a reduction in sediment transport efficiency, with little to no dependence on channel width. In contrast, a shear-stress partitioning effect cannot explain the slope ratio.

The theoretical framework presented in this paper is a first attempt to examine and test various physical mechanisms controlling the relationship between bedrock channel morphology and large boulders. We acknowledge two primary key future research questions emerging from our work. First, we have insufficient insights into the dynamics of bedload relating to sediment deflection in vicinity to boulders. Many of our model predictions may improve when the controls on the deflection length scale are better understood. Second, revealing the durability of boulders in bedrock channels is expected to promote understanding of the processes operating in the presence of boulders and the consequence on channel morphology.

#### **Author Contributions**

R.N., J.M.T. and L.G. conceived the study and developed the theory. R.N. collected the data, performed the analysis, and wrote the manuscript with input from all authors.

#### **Funding**

Funding

This research is supported by the Israel Science Foundation (grants 832/14 No. 562/19) and the NSF-BSF Foundation (grant 2018619). R.N. is supported by the Ben-Gurion University of the Negev "Hightech, Biotech & Chemotech" scholarship. Fieldwork was supported by GFZ.

#### **Conflict of interests**

The authors declare that they have no competing interests.

#### **Acknowledgments**

Wen-sheng Chen and Wen-Yen Chang are warmly thanked for supporting field logistics and permissions in Taroko National Park, Taiwan. We thank Jui-Ming Chang and Yu-Hsuan Yin for field assistance and fruitful discussions. We thank Tom Kaholi for field assistance and boulder digitization. Hagar Tevet and Guy Fisch are thanked for assisting in boulder digitization. Charles Shobe, Anne Voigtländer, and Joel Scheingross provided detailed comments on an earlier version of the manuscript.

## Appendix A: Slope Solution to the Shear-stress Partitioning effect

Here we solve the equation of shear-stress partitioning (Section 4.2.2) for the slope ratio. First, from geometry and continuity, it follows that (Turowski, 2021)

$$2Q \left( \frac{\tau}{g} \right) = QSW - K_V W^2 S^{\frac{1}{2}-\delta} \left( \frac{\tau}{g} \right)^{1+\delta} \quad (\text{A1})$$

For intermediate width, the term on the left-hand side of the equation can be neglected, and (A) can be solved for channel width

$$W = (g)^{\delta+1} \frac{QS^{\delta+0.5}}{K_V} \tau^{-(\delta+1)} \quad (\text{A2})$$

For a boulder-bed channel, Eq. (A2) can be rewritten as

$$W_b = (g)^{\delta+1} \frac{QS_b^{\delta+0.5}}{K_V} \tau_m^{-(\delta+1)} \quad (\text{A3})$$

Dividing (A3) by (A2)

$$\frac{W_b}{W} = \left( \frac{S_b}{S} \right)^{\delta+0.5} \left( \frac{\tau_m}{\tau} \right)^{-(\delta+1)} \quad (\text{A4})$$

From (27), it follows that

$$\frac{W_b}{W} = \left( \frac{\tau_{\text{red}}^*}{\tau^*} \right)^{-3/2} \quad (\text{A5})$$

Equating equations (A4) and (A5) and solving for the slope ratio

$$\frac{S_b}{S} = \left( \frac{\tau_m}{\tau} \right)^{\frac{\delta-0.5}{\delta+0.5}} \quad (\text{A6})$$

Finally, Eq. (2) is substituted into (A6) to yield a solution for the slope ratio as a function of boulder-concentration (Eq. 29).

## References

- Ancey, C., 2010, Stochastic modeling in sediment dynamics: Exner equation for planar bed incipient bed load transport conditions: *Journal of Geophysical Research: Earth Surface*, v. 115, p. 1–21, doi:10.1029/2009jf001260. Auel, C., Albayrak, I., Sumi, T., and Boes, R.M., 2017, Sediment transport in high-speed flows over a fixed bed: 2. Particle impacts and abrasion prediction: *Earth Surface Processes and Landforms*, v. 42, p. 1365–1383, doi:10.1002/esp.4128. Barry, J.J., Buffington, J.M., and King, J.G., 2004, A general power equation for predicting bed load transport rates in gravel bed rivers: *Water Resources Research*, v. 40, p. 1–22, doi:10.1029/2004WR003190. Bathurst, J.C., 1996, Field measurement of boulder flow drag: *Journal of Hydraulic Engineering*, v. 122, p. 167–169. Beer, A.R., and Turowski, J.M., 2015, Bedload transport controls bedrock erosion under sediment-starved conditions: *Earth Surface Dynamics*, v. 3, p. 291–309, doi:10.5194/esurf-3-291-2015. Beer, A.R., Turowski, J.M., and Kirchner, J.W., 2017, Spatial patterns of erosion in a

bedrock gorge: *Journal of Geophysical Research: Earth Surface*, p. 191–214, doi:10.1002/2016JF003850.

Bennett, G.L., Miller, S.R., Roering, J.J., and Schmidt, D.A., 2016, Landslides, threshold slopes, and the survival of relict terrain in the wake of the Mendocino Triple Junction: *Geology*, v. 44, p. 363–366, doi:10.1130/G37530.1.

Blom, A., Arkesteijn, L., Chavarrias, V., and Viparelli, E., 2017, The equilibrium alluvial river under variable flow and its channel-forming discharge: *Journal of Geophysical Research: Earth Surface*, v. 122, p. 1924–1948, doi:10.1002/2017JF004213.

Blom, A., Viparelli, E., and Chavarrias, V., 2016, The graded alluvial river: Profile concavity and downstream fining: *Geophysical Research Letters*, v. 43, p. 6285–6293, doi:10.1002/2016GL068898.

Bolla Pittaluga, M., Luchi, R., and Seminara, G., 2014, On the equilibrium profile of river beds: *Journal of Geophysical Research: Earth Surface*, v. 119, p. 317–332, doi:10.1002/2013JF002806.

Buffington, J.M., and Montgomery, D.R., 1997, A systematic analysis of eight decades of incipient motion studies, with special reference to gravel-bedded rivers: *Water Resources Research*, v. 33, p. 1993–2029, doi:10.1029/97WR03138.

Canovaro, F., Paris, E., and Solari, L., 2007, Effects of macro-scale bed roughness geometry on flow resistance: *Water Resources Research*, v. 43, p. 1–17, doi:10.1029/2006WR005727.

Carling, P.A., Hoffmann, M., and Blatter, A., 2002, Initial motion of boulders in bedrock channels: *Ancient Floods, Modern Hazards: Principles and Applications of Paleoflood Hydrology*, American Geophysical Union, Washington, DC., v. 5, p. 147–160.

Chiari, M., Friedl, K., and Rickenmann, D., 2010, A one-dimensional bedload transport model for steep slopes: *Journal of Hydraulic Research*, v. 48, p. 152–160, doi:10.1080/00221681003704087.

Cook, K.L., Andermann, C., Gimbert, F., Adhikari, B.R., and Hovius, N., 2018a, Glacial lake outburst floods as drivers of fluvial erosion in the Himalaya: *Science*, v. 57, p. 53–57.

Cook, K.L., Turowski, J.M., and Hovius, N., 2013, A demonstration of the importance of bedload transport for fluvial bedrock erosion and knickpoint propagation: *Earth Surface Processes and Landforms*, v. 38, p. 683–695, doi:10.1002/esp.3313.

Cook, K.L., Turowski, J.M., and Hovius, N., 2014, River gorge eradication by downstream sweep erosion: *Nature Geoscience*, v. 7, p. 682–686, doi:10.1038/ngeo2224.

Cook, K.L., Turowski, J.M., and Hovius, N., 2020, Width control on event-scale deposition and evacuation of sediment in bedrock-confined channels: *Earth Surface Processes and Landforms*, v. 45, p. 3702–3713, doi:10.1002/esp.4993.

Dadson, S.J. et al., 2003, Links between erosion, runoff variability and seismicity in the Taiwan orogen: *Nature*, v. 426, p. 648–651, doi:10.1038/nature02150.

Davis, W.M., 1902, Base level, grade and peneplain: *Journal of Geology*, v. 10, p. 77–111.

Dey, S., 2014, *Fluvial Hydrodynamics: Hydrodynamic and Sediment Transport Phenomena*: Springer.

Dey, S., Sarkar, S., Bose, S.K., Tait, S., and Castro-Organ, O., 2011, Wall-wake flows downstream of a sphere placed on a plane rough wall: *Journal of Hydraulic Engineering*, v. 137, p. 1173–1189, doi:10.1061/(asce)hy.1943-7900.0000441.

DiBiase, R. a., and Whipple, K.X., 2011, The influence of erosion thresholds and runoff variability on the relationships among topography, climate, and erosion rate: *Journal of Geophysical Research: Earth Surface*,

v. 116, p. 1–17, doi:10.1029/2011JF002095. DiBiase, R. a., Whipple, K.X., Heimsath, A.M., and Ouimet, W.B., 2010, Landscape form and millennial erosion rates in the San Gabriel Mountains, CA: *Earth and Planetary Science Letters*, v. 289, p. 134–144, doi:10.1016/j.epsl.2009.10.036. Dini, B., Bennett, G.L., Franco, A.M.A., Whitworth, M.R.Z., Cook, K.L., Senn, A., and Reynolds, J.M., 2021, Development of smart boulders to monitor mass movements via the Internet of Things: A pilot study in Nepal: *Earth Surface Dynamics*, v. 9, p. 295–315, doi:10.5194/esurf-9-295-2021. Einstein, H.A., 1950, The bed-load function for sediment transportation in open channel flows: USDA, Soil Conservation Service Tech. Bull. 1026, Washington, DC. Einstein, G.A., and Banks, R.B., 1950, Fluid resistance of composite roughness: *AGU*, v. 31, p. 603–610. Fernandez Luque, R., and Van Beek, R., 1976, Erosion and transport of bed-load sediment: *Journal of Hydraulic Research*, v. 14, p. 127–144, doi:10.1080/00221687609499677. Finnegan, N.J., Broudy, K.N., Nereson, A.L., Roering, J.J., Handwerker, A.L., and Bennett, G., 2019, River channel width controls blocking by slow-moving landslides in California’s Franciscan mélange: *Earth Surface Dynamics*, v. 7, p. 879–894, doi:10.5194/esurf-7-879-2019. Fuller, T.K., B., G.K., Sklar, L.S., and Paola, C., 2016, Lateral erosion in an experimental bedrock channel: The influence of bed roughness on erosion by bed load impacts Theodore: *Journal of Geophysical Research: Earth Surface*, v. 121, p. 1081–1105, doi:10.1002/2014JF003086. Gilbert, G.K., 1877, Report on the Geology of the Henry Mountains: US Government Printing Office. Hartshorn, K., Hovius, N., Dade, W.B., and Slingerland, R.L., 2002, Climate-driven bedrock incision in an active mountain belt: *Science*, v. 297, p. 2036–2038, doi:10.1126/science.1075078. Haviv, I., 2007, Mechanics, morphology and evolution of vertical knickpoints (waterfalls) along the bedrock channels of the Dead Sea western tectonic escarpment. Unpublished Dissertation, The Hebrew University of Jerusalem. He, C., Yang, C., and Turowski, J.M., 2021, The effect of roughness spacing and size on lateral deflection of bedload particles: *Water Resources Research*, doi:10.1029/2021wr029717. Huber, M.L., Lupker, M., Gallen, S.F., Christl, M., and Gajurel, A.P., 2020, Timing of exotic, far-traveled boulder emplacement and paleo-outburst flooding in the central Himalayas: *Earth Surface Dynamics*, v. 8, p. 769–787, doi:10.5194/esurf-8-769-2020. Johnson, J.P.L., 2017, Clustering statistics, roughness feedbacks, and randomness in experimental step-pool morphodynamics: *Geophysical Research Letters*, v. 44, p. 3653–3662, doi:10.1002/2016GL072246. Johnson, J.P.L., Whipple, K.X., and Sklar, L.S., 2010, Contrasting bedrock incision rates from snowmelt and flash floods in the Henry Mountains, Utah: *Bulletin of the Geological Society of America*, v. 122, p. 1600–1615, doi:10.1130/B30126.1. Johnson, J.P.L., Whipple, K.X., Sklar, L.S., and Hanks, T.C., 2009, Transport slopes, sediment cover, and bedrock channel incision in the Henry Mountains, Utah: *Journal of Geophysical Research: Earth Surface*, v. 114, p. 1–21, doi:10.1029/2007JF000862. Jouvét, G., Seguinot, J., Ivy-Ochs, S., and Funk, M., 2017, Modelling the diversion of erratic boulders by the Valais Glacier during the last glacial maximum: *Journal of Glaciology*, v. 63, p. 487–498, doi:10.1017/jog.2017.7. Kean, J.W., Staley, D.M., Lancaster, J.T., Rengers, F.K., Swanson, B.J., Coe, J.A., Hernandez,

J.L., Sigman, A.J., Allstadt, K.E., and Lindsay, D.N., 2019, Inundation, flow dynamics, and damage in the 9 January 2018 Montecito debris-flow event, California, USA: Opportunities and challenges for post-wildfire risk assessment: *Geosphere*, v. 15, p. 1140–1163, doi:10.1130/GES02048.1.

Lague, D., 2010, Reduction of long-term bedrock incision efficiency by short-term alluvial cover intermittency: *Journal of Geophysical Research: Earth Surface*, v. 115, p. n/a-n/a, doi:10.1029/2008JF001210.

Lague, D., 2014, The stream power river incision model: Evidence, theory and beyond: *Earth Surface Processes and Landforms*, v. 39, p. 38–61, doi:10.1002/esp.3462.

Lague, D., Hovius, N., and Davy, P., 2005, Discharge, discharge variability, and the bedrock channel profile: *Journal of Geophysical Research: Earth Surface*, v. 110, p. 1–17, doi:10.1029/2004JF000259.

Lamb, M.P., Dietrich, W.E., and Venditti, J.G., 2008, Is the critical Shields stress for incipient sediment motion dependent on channel-bed slope? *Journal of Geophysical Research*, v. 113, p. 1–20, doi:10.1029/2007JF000831.

Lane, E.W., 1955, The importance of fluvial morphology in hydraulic engineering. *Proceedings American Society of Civil Engineers*, v. 81, paper no. 745.

Lenzi, M.A., 2001, Step-pool evolution in the Rio Cordon, Northeastern Italy: *Earth Surface Processes and Landforms*, v. 26, p. 991–1008, doi:10.1002/esp.239.

Li, T., Fuller, T.K., Sklar, L.S., Gran, K.B., and Venditti, J.G., 2020, A Mechanistic Model for Lateral Erosion of Bedrock Channel Banks by Bedload Particle Impacts: *Journal of Geophysical Research: Earth Surface*, v. 125, doi:10.1029/2019JF005509.

Mackin, J.H., 1948, Concept of the graded river: *Geological Society of America Bulletin*, v. 59, p. 463–512, doi:10.1130/0016-7606(1948)59[463:COTGR]2.0.CO;2.

McKie, C.W., Juez, C., Plumb, B.D., Annable, W.K., and Franca, M.J., 2021, How Large Immobile Sediments in Gravel Bed Rivers Impact Sediment Transport and Bed Morphology: *Journal of Hydraulic Engineering*, v. 147, p. 04020096, doi:10.1061/(asce)hy.1943-7900.0001842.

Meyer-Peter, E., and Müller, R., 1948, Formulas for Bed-load transport: *Proceedings of the 2nd Meeting of the International Association of Hydraulic Research*, p. 39–64, doi:1948-06-07.

Montgomery, D.R., and Buffington, J.M., 1997, Channel-reach morphology in mountain drainage basins: *Bulletin of the Geological Society of America*, v. 109, p. 596–611, doi:10.1130/0016-7606(1997)109<0596:CRMIMD>2.3.CO;2.

Montgomery, D.R., and Gran, K.B., 2001, Downstream variations in the width of bedrock channels: *Water Resources Research*, v. 37, p. 1841–1846.

Nitsche, M., Rickenmann, D., Kirchner, J.W., Turowski, J.M., and Badoux, A., 2012, Macro-roughness and variations in reach-averaged flow resistance in steep mountain streams: *Water Resources Research*, v. 48, p. 1–16, doi:10.1029/2012WR012091.

Nitsche, M., Rickenmann, D., Turowski, J.M., Badoux, A., and Kirchner, J.W., 2011, Evaluation of bedload transport predictions using flow resistance equations to account for macro-roughness in steep mountain streams: *Water Resources Research*, v. 47, doi:10.1029/2011WR010645.

Pagliara, S., and Chiavaccini, P., 2006, Flow Resistance of rock chutes with protruding boulders: *Journal of Hydraulic Engineering*, v. 132, p. 545–552, doi:10.1061/(ASCE)0733-9429(2006)132:6(545).

Paola, C., and Voller, V.R., 2005, A generalized Exner equation for sediment mass balance: *Journal of Geophysical Research: Earth*

Surface, v. 110, p. 1–8, doi:10.1029/2004JF000274. Papanicolaou, A.N., and Kramer, C., 2006, The role of relative submergence on cluster microtopography and bedload predictions in mountain streams: River, Coastal and Estuarine Morphodynamics: RCEM 2005 - Proceedings of the 4th IAHR Symposium on River, Coastal and Estuarine Morphodynamics, v. 2, p. 1083–1086, doi:10.1201/9781439833896.ch117. Papanicolaou, A.N., Kramer, C.M., Tsakiris, A.G., Stoesser, T., Bomminayuni, S., and Chen, Z., 2012, Effects of a fully submerged boulder within a boulder array on the mean and turbulent flow fields: Implications to bedload transport: Acta Geophysica, v. 60, p. 1502–1546, doi:10.2478/s11600-012-0044-6. Papanicolaou, A.N., and Tsakiris, A.G., 2017, Boulder Effects on Turbulence and Bedload Transport (D. Tsutsumi & J. B. Laronne, Eds.): John Wiley & Sons Ltd. Published, 33–72 p., doi:10.1002/9781118971437.ch2. Papanicolaou, A.N.T., Tsakiris, A.G., Wyssmann, M.A., and Kramer, C.M., 2018, Boulder array effects on bedload pulses and depositional patches: Journal of Geophysical Research: Earth Surface, v. 123, p. 2925–2953, doi:10.1029/2018JF004753. Parker, G., 1979, Hydraulic geometry of active gravel rivers: Journal of the Hydraulics Division, v. 105, p. 1185–1201. Parker, G., 1978, Self-formed straight rivers with equilibrium banks and mobile bed. Part 2. The gravel river: Journal of Fluid mechanics, v. 89, p. 127–146. Phillips, C.B., and Jerolmack, D.J., 2016, Self-organization of river channels as a critical filter on climate signals: Science, v. 352, p. 694–697, doi:10.1126/science.aad3348. Polvi, L.E., 2021, Morphodynamics of boulder-bed semi-alluvial streams in Northern Fennoscandia: A flume experiment to determine sediment self-organization: Water Resources Research, v. 57, doi:10.1029/2020WR028859. Prancevic, J.P., and Lamb, M.P., 2015, Unraveling bed slope from relative roughness in initial sediment motion: Journal of Geophysical Research: Earth Surface: Earth Surface, v. 120, p. 474–489, doi:10.1002/2014JF003323. Rickenmann, D., 2001, Comparison of bed load transport in torrents and gravel bed streams: Water Resources Research, v. 37, p. 3295–3305. Rickenmann, D., and Recking, A., 2011, Evaluation of flow resistance in gravel-bed rivers through a large field data set: Water Resources Research, v. 47, doi:10.1029/2010WR009793. Royden, L., and Perron, J.T., 2013, Solutions of the stream power equation and application to the evolution of river longitudinal profiles: Journal of Geophysical Research: Earth Surface, v. 118, p. 497–518, doi:10.1002/jgrf.20031. Schneider, J.M., Rickenmann, D., Turowski, J.M., Bunte, K., and Kirchner, J.W., 2015a, Applicability of bed load transport models for mixed-size sediments in steep streams considering macro-roughness: Water Resources Research, v. 51, p. 5260–5283, doi:10.1002/2014WR016417. Schneider, J.M., Rickenmann, D., Turowski, J.M., and Kirchner, J.W., 2015b, Self-adjustment of stream bed roughness and flow velocity in a steep mountain channel: Water Resources Research, v. 51, p. 7839–7859, doi:10.1002/2015WR016934. Schumm, S.A., and Parker, R. S., 1973, Implications of complex response of drainage systems for Quaternary alluvial stratigraphy: Nat. Phys. Sci., v. 243, p. 99–100, doi:https://doi.org/10.1038/physci243099a0. Seizilles, G., Lajeunesse, E., Devauchelle, O., and Bak, M., 2014, Cross-stream diffusion in bedload transport:

Physics of Fluids, v. 26, doi:10.1063/1.4861001.Shobe, C.M., Bennett, G.L., Tucker, G.E., Roback, K., Miller, S.R., and Roering, J.J., 2020, Boulders as a lithologic control on river and landscape response to tectonic forcing at the Mendocino triple junction: Geological Society of America Bulletin, p. 1–16, doi:10.1130/B35385.1.Shobe, C.M., Tucker, G.E., and Anderson, R.S., 2016, Hillslope-derived blocks retard river incision: Geophysical Research Letters, v. 43, p. 5070–5078, doi:10.1002/2016GL069262.1.Shobe, C.M., Tucker, G.E., and Rossi, M.W., 2018, Variable-threshold behavior in rivers arising from hillslope-derived blocks: Journal of Geophysical Research: Earth Surface, v. 123, p. 1–27, doi:10.1029/2017JF004575.Shobe, C.M., Turowski, J.M., Nativ, R., Glade, R.C., Bennett, G.L., and Dini, B., 2021, The role of infrequently mobile boulders in modulating landscape evolution and geomorphic hazards: Earth-Science Reviews, v. 220, p. 103717, doi:10.1016/j.earscirev.2021.103717.Sklar, L.S., and Dietrich, W.E., 2004, A mechanistic model for river incision into bedrock by saltating bed load: Water Resources Research, v. 40, p. 1–22, doi:10.1029/2003WR002496.Sklar, L., and Dietrich, W.E., 1998, River longitudinal profiles and bedrock incision models: Stream power and the influence of sediment supply, *in* Rivers Over Rock: Fluvial Processes in Bedrock Channels, Geophysical Monograph Series 107, p. 237–260, doi:10.1029/GM107.Sklar, L.S., and Dietrich, W.E., 2006, The role of sediment in controlling steady-state bedrock channel slope: Implications of the saltation-abrasion incision model: Geomorphology, v. 82, p. 58–83, doi:10.1016/j.geomorph.2005.08.019.Thaler, E.A., and Covington, M.D., 2016, The influence of sandstone caprock material on bedrock channel steepness within a tectonically passive setting: Buffalo National River Basin, Arkansas, USA: Journal of Geophysical Research: Earth Surface, v. 121, p. 1635–1650, doi:10.1002/2015JF003771.Tsakiris, A.G., Papanicolaou, A.N.T., Hajimirzaie, S.M., and Buchholz, J.H.J., 2014, Influence of collective boulder array on the surrounding time-averaged and turbulent flow fields: Journal of Mountain Science, v. 11, p. 1420–1428, doi:10.1007/s11629-014-3055-8.Turowski, J.M., 2018, Alluvial cover controlling the width, slope and sinuosity of bedrock channels: Earth Surface Dynamics, v. 6, p. 29–48, doi:10.5194/esurf-6-29-2018.Turowski, J.M., 2020a, Mass balance, grade, and adjustment timescales in bedrock channels: Earth Surface Dynamics, v. 8, p. 103–122, doi:10.5194/esurf-2019-47.Turowski, J.M., 2020b, Mass balance, grade, and adjustment timescales in bedrock channels: Earth Surface Dynamics, v. 8, p. 103–122, doi:10.5194/esurf-8-103-2020.Turowski, J.M., 2021, Upscaling sediment-flux-dependent fluvial bedrock incision to long timescales: Journal of Geophysical Research: Earth Surface, doi:10.1029/2020jf005880.Turowski, J.M., and Hodge, R., 2017, A probabilistic framework for the cover effect in bedrock erosion: Earth Surface Dynamics, v. 5, p. 311–330, doi:10.5194/esurf-5-311-2017.Turowski, J.M., Hovius, N., Lague, D., Hsieh, M.-L., and Men-Chiang, C., 2008, Distribution of erosion across bedrock channels: Earth Surface Processes and Landforms, v. 33, p. 353–363, doi:10.1002/esp.1559.Turowski, J.M., Lague, D., and Hovius, N., 2007, Cover effect in bedrock abrasion: A new derivation and its implications for the modeling of bedrock channel morphology: Journal of Geophysical Research: Earth

Surface, v. 112, p. 1–16, doi:10.1029/2006JF000697. Turowski, J.M., Lague, D., and Hovius, N., 2009a, Response of bedrock channel width to tectonic forcing: Insights from a numerical model, theoretical considerations, and comparison with field data: *Journal of Geophysical Research: Solid Earth*, v. 114, p. 1–16, doi:10.1029/2008JF001133. Turowski, J.M., Yager, E.M., Badoux, A., Rickenmann, D., and Molnar, P., 2009b, The impact of exceptional events on erosion, bedload transport and channel stability in a step-pool channel: *Earth Surface Processes and Landforms*, v. 34, p. 155–161, doi:10.1002/esp. Whipple, K. X. (2004). Bedrock rivers and the geomorphology of active orogens. *Annual Review of Earth and Planetary Sciences*, 32, 151– 185. Whipple, K.X., and Tucker, G.E., 1999, Dynamics of the stream-power river incision model: Implications for height limits of mountain ranges, landscape response timescales, and research needs: *Journal of Geophysical Research*, v. 104, p. 17661, doi:10.1029/1999JB900120. Whitbread, K., Jansen, J., Bishop, P., and Attal, M., 2015, Substrate, sediment, and slope controls on bedrock channel geometry in postglacial streams: *Journal of Geophysical Research F: Earth Surface*, v. 120, p. 779–798, doi:10.1002/2014JF003295. Wiberg, P.L., and Smith, J.D., 1991, Velocity distribution and bed roughness in high-gradient streams: *Water Resources Research*, v. 27, p. 825–838, doi:10.1029/90WR02770. Wilson, A., Hovius, N., and Turowski, J.M., 2013, Geomorphology Upstream-facing convex surfaces: Bedrock bedforms produced by fluvial bedload abrasion: *Geomorphology*, v. 180–181, p. 187–204, doi:10.1016/j.geomorph.2012.10.010. Wobus, C., Whipple, K.X., Kirby, E., Snyder, N., Johnson, J., Spyropolou, K., Crosby, B., and Sheehan, D., 2006, Tectonics from topography: procedures, promise, and pitfalls: *Geological Society of America Special Paper*, v. 398, p. 55–74, doi:10.1130/2006.2398(04). Wong, M., and Parker, G., 2006, Reanalysis and correction of bed-load relation of Meyer-Peter and Müller using their own database: *Journal of Hydraulic Engineering*, v. 132, p. 1159–1168, doi:10.1061/(ASCE)0733-9429(2006)132:11(1159). Yager, E.M., Kirchner, J.W., and Dietrich, W.E., 2007, Calculating bed load transport in steep boulder bed channels: *Water Resources Research*, v. 43, p. 1–24, doi:10.1029/2006WR005432. Yanites, B.J., 2018, The dynamics of channel slope, width, and sediment in actively eroding bedrock river systems: *Journal of Geophysical Research: Earth Surface*, v. 123, p. 1504–1527, doi:10.1029/2017JF004405. Zhou, Z. et al., 2017, Is “Morphodynamic Equilibrium” an oxymoron? *Earth-Science Reviews*, v. 165, p. 257–267, doi:10.1016/j.earscirev.2016.12.002.